

Image-based drug screen identifies HDAC inhibitors as novel Golgi disruptors synergizing with JQ1

Mathieu Gendarme^a, Jan Baumann^a, Tatiana I. Ignashkova^a, Ralph K. Lindemann^b, and Jan H. Reiling^{a,*}

^aBioMed X Innovation Center, 69120 Heidelberg, Germany; ^bTranslational Innovation Platform Oncology, Merck Biopharma, Merck KGaA, 64293 Darmstadt, Germany

ABSTRACT The Golgi apparatus is increasingly recognized as a major hub for cellular signaling and is involved in numerous pathologies, including neurodegenerative diseases and cancer. The study of Golgi stress-induced signaling pathways relies on the selectivity of the available tool compounds of which currently only a few are known. To discover novel Golgi-fragmenting agents, transcriptomic profiles of cells treated with brefeldin A, golgicide A, or monensin were generated and compared with a database of gene expression profiles from cells treated with other bioactive small molecules. In parallel, a phenotypic screen was performed for compounds that alter normal Golgi structure. Histone deacetylase (HDAC) inhibitors and DNA-damaging agents were identified as novel Golgi disruptors. Further analysis identified HDAC1/HDAC9 as well as BRD8 and DNA-PK as important regulators of Golgi breakdown mediated by HDAC inhibition. We provide evidence that combinatorial HDACi/(+)-JQ1 treatment spurs synergistic Golgi dispersal in several cancer cell lines, pinpointing a possible link between drug-induced toxicity and Golgi morphology alterations.

Monitoring Editor

Akihiko Nakano
RIKEN

Received: Mar 20, 2017

Revised: Oct 17, 2017

Accepted: Oct 17, 2017

INTRODUCTION

The Golgi apparatus is a dynamic, membranous organelle involved in processing, sorting, and transport of proteins and lipids, thus playing an essential role in cellular homeostasis. In mammalian cells under normal conditions, the Golgi is organized as a compacted peri-nuclear stack of membranes (cisternae); however, this mor-

phology is required to undergo immense structural changes to fulfill its various functions, including the maintenance of cell polarity, wound healing (Yadav *et al.*, 2009), and cell proliferation (Sütterlin *et al.*, 2002). In addition to its role in protein sorting and trafficking, the Golgi also serves as an important signaling platform (Cancino and Luini, 2013) that, for instance, can support oncogenic rat sarcoma (RAS) signaling (Chiu *et al.*, 2002) and is itself regulated by a vast network of signaling proteins (Chia *et al.*, 2012). Deregulation of Golgi morphology has been recognized as an important contributor to oncogenesis (Petrosyan, 2015). For instance, the Golgi morphology regulator GOLPH3 is amplified in many different cancer types (lung, ovarian, breast, pancreatic, prostate, and skin) (Xi *et al.*, 2016). GOLPH3 has been shown to regulate mTOR signaling and proliferation (Scott *et al.*, 2009; Zeng *et al.*, 2012) and metastasis, as well as malignant secretion (Halberg *et al.*, 2016), and can be directly phosphorylated by the DNA damage repair protein DNA-PK (Farber-Katz *et al.*, 2014). Golgi fragmentation occurs under various stress conditions, suggesting the existence of conserved pathways that regulate Golgi morphology (Machamer, 2015). Progress has been made in defining Golgi stress-responsive pathways triggered in response to a small number of Golgi-dispersing compounds, such as brefeldin A (BFA), golgicide A (GCA), or monensin (Fujiwara *et al.*, 1988; Pan *et al.*, 2008; Sáenz *et al.*, 2009;

This article was published online ahead of print in MBoc in Press (<http://www.molbiolcell.org/cgi/doi/10.1091/mbc.E17-03-0176>) on October 26, 2017.

Author contributions: M.G., J.B., and J.H.R. conceived the study. R.K.L. provided valuable advice. M.G., J.B., and T.I. performed the experiments and analyzed the data. M.G., J.B., and J.H.R. wrote the article.

*Address correspondence to: Jan H. Reiling (reiling@bio.mx).

Abbreviations used: ARFs, ADP-ribosylation factors; BCP, bromodomain-containing protein; BET, bromodomain and extraterminal; BFA, brefeldin A; DDR, DNA damage response; ER, endoplasmic reticulum; GCA, golgicide A; HAT(i), histone acetyl transferase (inhibitor); HDAC(i), histone deacetylase (inhibitor); IF, immunofluorescence; LINCS, Library of Integrated Network-based Cellular Signatures; MON, monensin; Pano., Panobinostat; RNAi, RNA interference; SAHA, suberonyl-hydroxamic acid; TEM, transmission electron microscopy.

© 2017 Gendarme *et al.* This article is distributed by The American Society for Cell Biology under license from the author(s). Two months after publication it is available to the public under an Attribution–Noncommercial–Share Alike 3.0 Unported Creative Commons License (<http://creativecommons.org/licenses/by-nc-sa/3.0>).

“ASCB®,” “The American Society for Cell Biology®,” and “Molecular Biology of the Cell®” are registered trademarks of The American Society for Cell Biology.

Oku *et al.*, 2011; Reiling *et al.*, 2013; Taniguchi *et al.*, 2015; Ignashkova *et al.*, 2017); however, the elucidation of potential Golgi stress signaling pathways and their impact on health and disease would likely benefit from the identification and use of additional reagents that interfere with Golgi homeostasis.

Lysine acetylation is an important posttranslational modification which is regulated in an antagonistic fashion by histone acetyltransferases (HATs) and histone deacetylases (HDACs). The human HDAC family consists of 18 members that are subdivided into the mainly nuclear localized class I (HDAC1, 2, 3, 8), the nuclear and cytoplasmically localized class IIa (HDAC 4, 5, 7, 9), and the cytoplasmic class IIb (HDAC6, 10). In addition, the poorly understood HDAC11 is the sole member of class IV. The activity of classes I, II, and IV HDACs are zinc ion (Zn^{2+}) dependent. The catalytically different class III (SIRT1-7) requires a nicotinamide adenine dinucleotide for their enzymatic activity. HDACs are involved in fundamental cellular processes, such as the regulation of gene expression (Grunstein, 1997), cell migration (Mottet *et al.*, 2007), and DNA replication (Stengel and Hiebert, 2015). HDACs are overexpressed in several cancer types, including lung, gastric, and ovarian cancers (Bartling *et al.*, 2005; Song *et al.*, 2005; Kha-bele *et al.*, 2007), and efforts have been made to exploit this fact for anti-tumor therapy. To date, four small molecule HDAC inhibitors are FDA approved to treat patients suffering from cutaneous T-cell lymphoma (Vorinostat, approved in 2006, and Romidepsin, approved in 2009) (Mann *et al.*, 2007; Hughes, 2010), refractory peripheral T-cell lymphoma (Belinostat, approved 2014) (Lee *et al.*, 2015) and multiple myeloma (Panobinostat, approved in 2015) (Bailey *et al.*, 2015), with many more compounds still in clinical development (Manal *et al.*, 2016). HDACis also show beneficial effects in other disease settings, including neurodegeneration, inflammation, and cardiovascular diseases (Falkenberg and Johnstone, 2014; Yoon and Eom, 2016). It is estimated that ~8–20% of genes are transcriptionally regulated by HDAC-mediated modification of histone tails (Peart *et al.*, 2005; Zhang and Zhong, 2014). In addition, the biological actions of HDACs have been extended from the regulation of histone acetylation to an array of other biological effects, mediated by the deacetylation of nonhistone proteins including transcription factors, cell cycle regulators, DNA repair factors, and metabolic enzymes (Xu *et al.*, 2007; Choudhary *et al.*, 2009; Witt *et al.*, 2009; Zhao *et al.*, 2010). Moreover, HDACi treatment can lead to reactive oxygen species (ROS) generation, thereby contributing to proapoptotic signaling (Falkenberg and Johnstone, 2014).

Here we have used two intersecting approaches to uncover small molecules that cause Golgi dispersal. On one hand, we have performed transcriptomics using three well-described Golgi-dispersing tool compounds to identify gene signatures associated with Golgi disintegration. We subsequently compared these gene expression profiles to the Library of Integrated Network-based Cellular Signatures (LINCS) L1000 database to identify compounds that induce similar gene expression profiles. On the other hand, we developed an image-based screening platform for Golgi structure alterations that led to the identification of HDACis, DNA-damaging agents and inhibitors of transcription as novel inducers of Golgi scattering. We further utilized this platform to identify HDAC1/HDAC9 as well as BRD8 and DNA-PK as major regulators of Golgi morphology. Finally, we found that multiple cancer cell lines display enhanced Golgi dispersal on combinatorial treatment of the bromodomain inhibitor (+)-JQ1 and HDAC inhibitors, which was associated with synergistic cell death.

RESULTS

Transcriptomics and connectivity map analysis of Golgi-disrupting compounds

In an effort to find new Golgi morphology modulators, we performed gene expression profiling of A549 cells treated with brefeldin A (BFA), golgicide A (GCA), or monensin (MON) using DNA microarrays. All three of these small molecules have been previously described to induce Golgi fragmentation as demonstrated by immunofluorescence experiments using several Golgi markers (Fujiwara *et al.*, 1988; Pan *et al.*, 2008; Sáenz *et al.*, 2009; van der Linden *et al.*, 2010; Chia *et al.*, 2012; Reiling *et al.*, 2013). The gene signature associated with each drug was used to query the LINCS L1000 database, a large-scale multi-center collaborative project to catalogue gene expression profiles of a multitude of conditions, similar to the original Connectivity Map (CMap) project but far more comprehensive (Lamb, 2006). During the revision of this article, the LINCS resource was replaced by the web application clue.io. The program compares the input gene signature to the database of gene expression signatures and outputs a list of compounds with connectivity scores that range from –100 to 100, indicating complete correlation (100) or complete anti-correlation (–100) of the two gene expression signatures in a panel of four different cell lines. A high positive connectivity score indicates that the corresponding compound induced a similar expression profile to that of the query signature. Compounds that entail similar transcriptional responses are likely to share a common mechanism of action (Scherf *et al.*, 2000; Lamb, 2007; Hu and Agarwal, 2009; Iorio *et al.*, 2009, 2010). To facilitate the analysis and downstream efforts, we focused our analysis on the top 50 correlated compounds (of a total of 2974 compounds) (Figure 1). As expected, the analysis revealed a strong correlation between all three of our query compounds (BFA, GCA, and MON) and the L1000 signature for brefeldin-a, indicating that the results are biologically meaningful. The second-highest scoring compound was AG-1478/tyrphostin, a compound that was originally described as an epidermal growth factor receptor (EGFR) inhibitor but was also shown to induce Golgi fragmentation in a manner similar to BFA (Pan *et al.*, 2008; van der Linden *et al.*, 2010). The gene expression profiling data also revealed high similarity between our query Golgi disruptors and several DNA damage-inducing agents, the latter of which were enriched in the top 50 hit list (5/50 of 30 DNA damage inducers in 2974 compounds, $p < 1.40 \times 10^{-4}$; see *Material and Methods*). A recent study reported that the DNA double-strand-break inducers doxorubicin, camptothecin, or ionizing radiation induce Golgi dispersal (Farber-Katz *et al.*, 2014). Our analysis of the L1000 database suggests that these properties extend also to DNA cross-linkers and additional topoisomerase inhibitors. Another striking finding of our analysis was the enrichment of HDACis in the top 50 correlated compounds (8/50 of 30 HDAC inhibitors in 2974 compounds, $p < 1.58 \times 10^{-8}$), none of which has previously been described to alter Golgi morphology.

Image-based screen identifies HDAC inhibitors and DNA damage inducers as Golgi disruptors

In a parallel approach to our transcriptomic analysis coupled to the interrogation of the LINCSCLOUD resource, we screened a custom-assembled library of 307 compounds (see *Materials and Methods*) using a fluorescence-based, high-content imaging platform, which allowed us to test whether our bioinformatics approach accurately predicted novel Golgi disruptors (Figure 2A). To this end, A549 cells were incubated in the presence of each test compound for 72 h before fixation. We subsequently stained the nucleus (Hoechst) to identify the seed region, the *cis*-Golgi (GM130) to quantify the Golgi

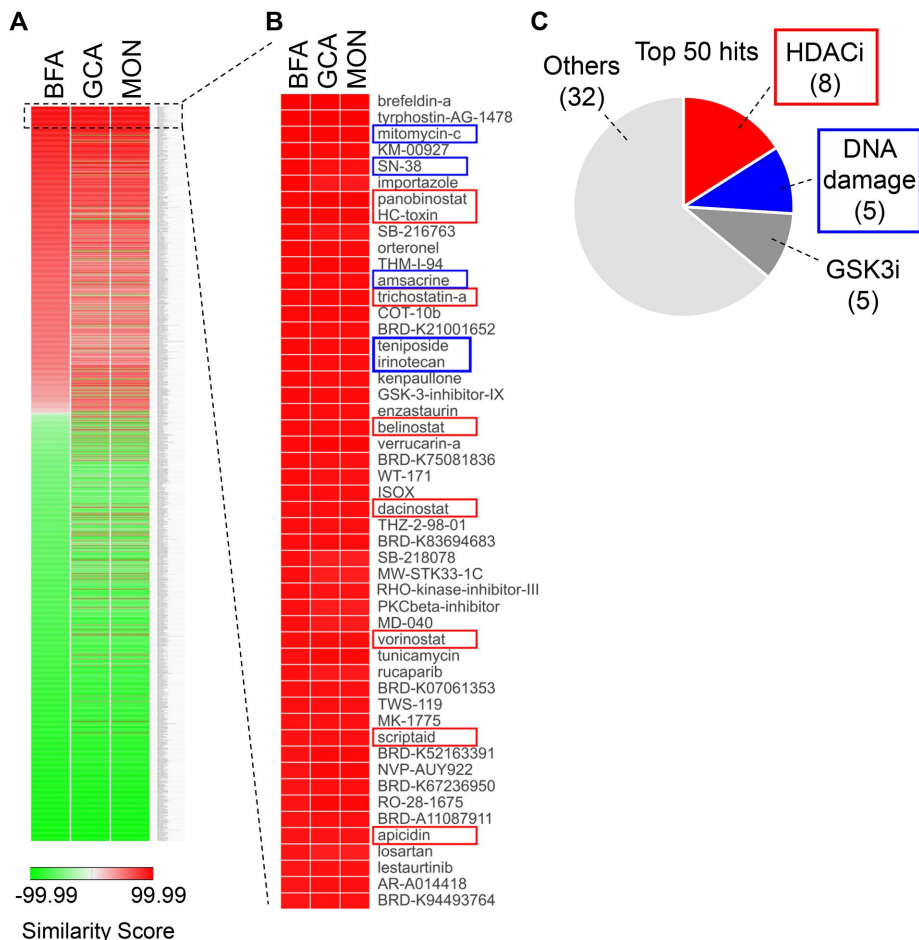


FIGURE 1: Connectivity map analysis of classical Golgi-fragmenting drugs predicts HDAC inhibitors and DNA-damaging agents as compounds with a similar mode of action. The gene expression signatures of A549 cells treated for 20 h with 71 nM BFA, 5 μ M GCA, or 10 μ M monensin were determined and used to query the LINCS L1000 database to identify compounds with similar gene expression profiles. (A) Heat map representation of all the gene expression signatures in the L1000 database and their connectivity scores in comparison with our own BFA, GCA, and monensin input expression profiles. The data were sorted based on the similarity score for BFA. (B) Detailed view of the top 50 correlations identified in this analysis and sorted by their similarity to the BFA profile. Blue boxes indicate DNA-damaging agents; red boxes indicate HDAC inhibitors. (C) Pie chart summarizing the compounds in the top 50 hit list.

area, the actin cytoskeleton (phalloidin) to evaluate cell size and morphology, and GRP78 to assess endoplasmic reticulum (ER) stress induction. Images from 20 fields per well were acquired for each condition in triplicate (i.e., 60 fields in total), enabling the quantification of ~1500 cells for each condition. The Golgi area was defined as the proportion of each cell in which GM130 signal can be detected. The screening set included several positive control compounds known to disperse the Golgi, such as BFA (Fujiwara *et al.*, 1988), nocodazole (Turner and Tartakoff, 1989), and doxorubicin (Farber-Katz *et al.*, 2014). Of all compounds tested, 107 caused a significant increase in the Golgi area (Figure 2, B and C). The observed increase in Golgi area correlated with a corresponding decrease in cell counts (Figure 2C), indicating a potential link between loss of Golgi apparatus integrity and cell viability (Ignashkova *et al.*, 2017). We set the cutoff for the hit selection at a 1.5-fold increase of the Golgi area compared with the vehicle control, because this number corresponded to the smallest significant Golgi-dispersing fold change obtained from the replicates of cells treated with 40 nM BFA. To minimize the inclusion of false-positive candidates, only

other than doxorubicin and camptothecin, as well as anti-metabolites. Of the eight HDAC inhibitors included in our screen, all but one (Entinostat) of which are pan-HDAC inhibitors (Pracinostat, Givinostat, Trichostatin A, 4-Iodo-SAHA, Oxamflatin, Vorinostat [SAHA], and Scriptaid), caused significant Golgi dispersal, thereby identifying HDAC inhibitors as novel Golgi disruptors (Figure 2, C and D). Entinostat was reported to display higher selectivity toward HDAC1 and HDAC3 (Hu *et al.*, 2003; Hess-Stumpp *et al.*, 2007; Bieliauskas and Pflum, 2008; Khan *et al.*, 2008). Unlike the control compounds BFA, AMF-26, GCA, or monensin, neither of the DNA damage inducers nor the HDACis caused noticeable up-regulation of the ER stress marker GRP78 (Figure 2D). Taken together, these results strongly suggest that HDAC activity is involved in the regulation of Golgi morphology.

Effects of additional HDACis and genetic HDAC depletion on Golgi structure

We next tested two additional HDAC inhibitors that were not part of the primary screen. First, we checked Panobinostat (LBH-589)

those compounds of which at least two of the three replicates displayed a Golgi area above the cutoff of 1.5 were selected as "true" hits. Our final hit list contained 20 compounds, including the eight positive controls. Thus, our screen identified 12 novel Golgi-dispersing compounds, which are mainly part of two compound classes: DNA damage inducers and HDAC inhibitors, thereby corroborating the predicted results from our *in silico* analysis. The general CDK inhibitor Flavopiridol, which acts as a transcription inhibitor and is in clinical development as an anti-tumor agent (Zeidner and Karp, 2015), was also found to disrupt the Golgi (Figure 2D). Among the DNA damage inducers, Bleomycin, a DNA single- and double-strand-break inducer (Ewig and Fornace, 1976), and the nucleoside analog Gemcitabine (Hertel *et al.*, 1990; Hecht, 2000) were identified as novel Golgi-fragmenting agents. While not part of the original screen, we also tested several other DNA damage-inducing agents, including irinotecan, teniposide, etoposide, mitomycin-c, cisplatin, 5-fluorouracil (5-FU), and hydroxyurea, all of which induced Golgi dispersal (Supplemental Figure S1). Interestingly, without exception, we found that DNA damage-inducing agents caused significant increases in cell size concomitantly with structural reorganization of the Golgi, a phenotype that, to our knowledge, has not been described previously (Figure 2D and Supplemental Figure S1). In most other cases, Golgi-dispersing agents had no effect or were associated with cell size decreases. Our results therefore significantly extend the panel of previously reported DNA-damaging drugs, which cause double-strand breaks and fragment the Golgi (Farber-Katz *et al.*, 2014), to DNA cross-linkers, additional topoisomerase inhibitors

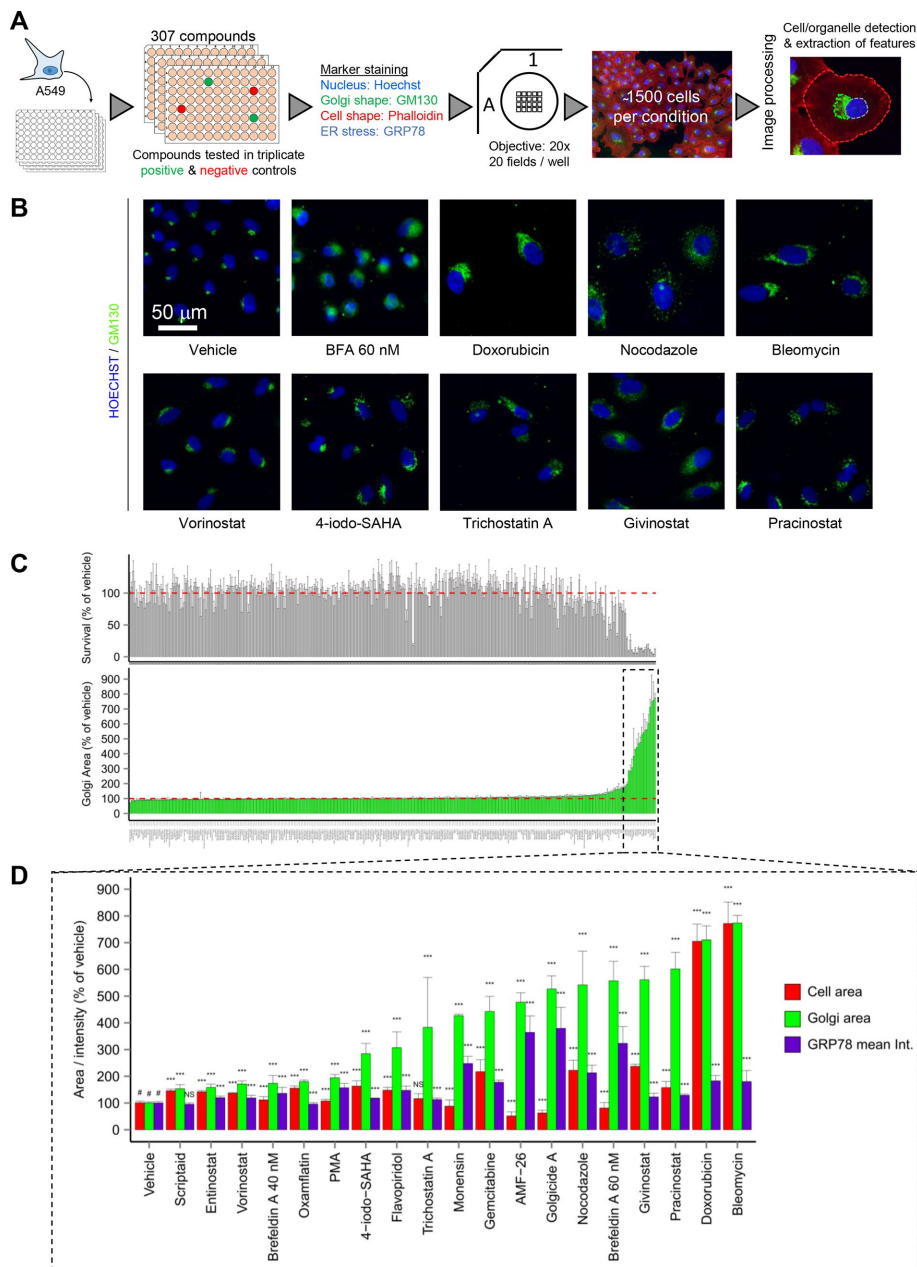


FIGURE 2: Image-based chemical compound screen identifies HDAC inhibitors and DNA-damaging agents as novel Golgi-dispersing compounds. To identify novel compounds that modulate Golgi morphology, a screening platform was established. (A) Screening pipeline including cell seeding (A549 cells), treatment with compound library, staining for the *cis*-Golgi (GM130), the nucleus (Hoechst), the ER stress marker (GRP78), cytoplasm (Phalloidin), and image acquisition and processing. (B) Representative images of the negative control (vehicle-treated cells) as well as positive controls (BFA, doxorubicin, and nocodazole) and newly discovered Golgi-fragmenting drugs (Bleomycin, Vorinostat, 4-iodo-SAHA, Trichostatin A, Givinostat, and Pracinostat) are displayed. (C) Following image analysis, to exclude potential plate effects, the Golgi area of cells treated with the chemical library was normalized to the vehicle-treated sample present within the same plate. The corresponding survival ratios of treated cells are also shown. (D) Detailed view of compounds are shown, of which at least two of three replicates caused a ≥ 1.5 -fold increase in Golgi area. The compound panel includes positive controls and novel Golgi-fragmenting compounds, which were selected for further investigation. *** $p < 0.001$ vs. #; see *Materials and Methods*.

because of its clinical prevalence and potency in the nanomolar range (Atadja, 2009; Laubach *et al.*, 2015; Nervi *et al.*, 2015; Manal *et al.*, 2016). Strikingly, Panobinostat treatment of A549 cells led to similar changes in Golgi architecture as the other HDACis

(Figure 3A). To evaluate ultrastructural alterations, Golgi morphology of A549 cells following Panobinostat treatment was assessed by transmission electron microscopy (TEM). Multiple sections of HDACi-treated cells revealed disorganized Golgi membranes and an expanded area covered by distinctively altered Golgi compartments displaying an enhanced presence of many large vesicular and tubular structures potentially representing dilated cisternae and or vesicles not observed in control cells. Unlike BFA, Panobinostat treatment did not cause an increased formation of lipid droplets, suggesting that both compounds have different metabolic effects (Supplemental Figure S2A). Tubastatin A was also tested because of its specificity toward HDAC6 (Butler *et al.*, 2010), which is known to regulate microtubule dynamics through the deacetylation of tubulin (Hubbert *et al.*, 2002). Interestingly, Tubastatin A did not trigger an increase in Golgi area comparable to other HDACis, despite the use of high drug concentrations (Figure 3A). Of note, all of the HDACis evaluated in this study induced an increase in cellular pan-acetyl lysine levels with the concentrations used in our screen and follow-up experiments (Figure 3A). Most prominent were acetylated lysine signals in the range of 10–15 kDa, a molecular weight range in which histones are expected to be detected. Only Tubastatin A treatment resulted in an increase in acetylated lysine signal at a molecular weight of around 50–55 kDa, at which size a signal for tubulin is to be expected (Figure 3A). These data suggest that either simultaneous inhibition of multiple HDACs and/or specifically HDAC1/3, but not HDAC6, may trigger Golgi disintegration. Further, we conclude that the regulation of microtubule dynamics via acetylation is not involved in this HDACi-mediated Golgi dispersal. To more broadly test whether total cellular levels of acetylated lysines impact the extent of pharmacologically induced Golgi disruption, A549 cells were cotreated with the histone acetyltransferase (HAT) inhibitor (HATI) CBP300 to reduce acetylation and BFA or HDACis, respectively. Interestingly, the addition of CBP300 suppressed to a certain extent Golgi disintegration induced by both BFA or Panobinostat treatment alone (Supplemental Figure S2B). In the case of Panobinostat, this partial suppression of Golgi dispersal was indeed associated with reduced levels of lysine acetylation (Supplemental Figure S2C). A time-course experiment of A549 cells treated with Panobinostat revealed that, unlike BFA, which is able to completely disperse the Golgi structure within minutes (Sciaky *et al.*, 1997), the extent of HDACi treatment-induced

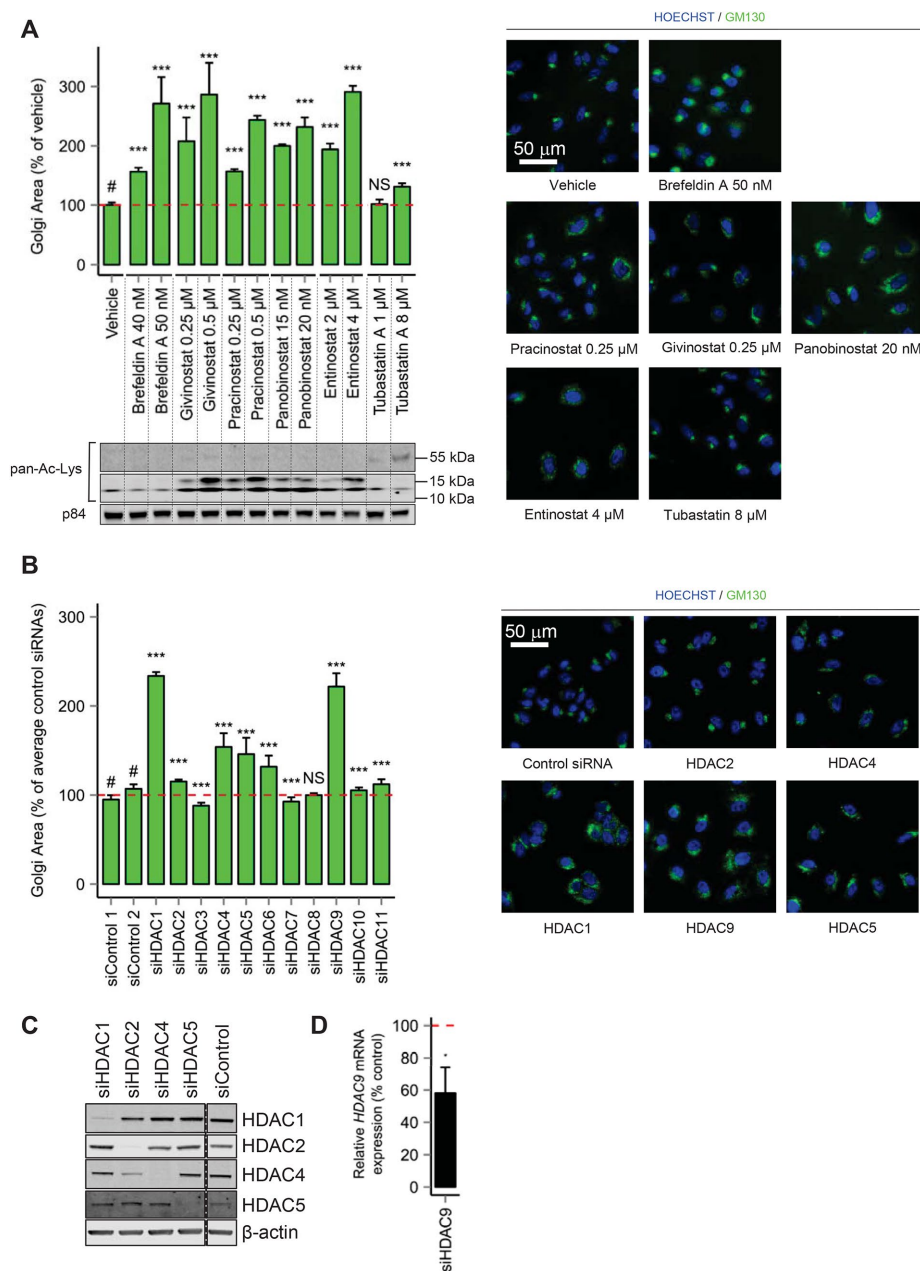


FIGURE 3: Effects of individual HDAC depletion and additional HDACis on Golgi structure. The HDACis identified in the screen in addition to Panobinostat (pan-HDAC), Entinostat (HDAC1i and HDAC3i), and Tubastatin (HDAC6i) were tested for their ability to disrupt the Golgi. (A) Quantification of immunofluorescence stainings of Golgi area of A549 cells treated with the indicated chemicals for 72 h. Representative images of the individual compounds are shown on the right. The levels of acetylated lysines were evaluated for each treatment condition by immunoblotting. Pictures of one representative experiment of three independent experiments are displayed. The levels of acetylated lysines were assessed by immunoblotting for each treatment condition. (B) Individual HDACs were depleted from A549 cells using siRNA; 48 h posttransfection Golgi area alterations were evaluated via immunofluorescence. (C, D) Knockdown efficiency was tested 48 h posttransfection for the indicated genes by Western blot (C) or qRT-PCR (D). (C) HDAC knockdown and siControl lysates were run on the same gel; dashed line in blot indicates where unrelated samples were cropped out of the image. *** $p < 0.001$ vs. # or control siRNA; see *Materials and Methods*.

Golgi dispersal increased over the course of 72 h, showing only a minor impact on Golgi structure and viability after 24 h, which were, however, significantly further enhanced (Golgi area) or decreased (viability), respectively, over the following 24–48 h (Supplemental

Panobinostat treatment are consistently and noticeably rescued in the presence of the pan caspase inhibitor Z-VAD-FMK unlike with BFA (Figure 4A). Thus, the absence of cell death after 24 h of Panobinostat treatment (Supplemental Figure S2D) plus the lack of

Figure S2D). Thus, compared with BFA treatment the effects of HDACi on Golgi architecture are discernible only after substantially longer drug incubation times.

To genetically corroborate the results obtained with the HDACi hit compounds identified in the high-content screen and to pinpoint the relevant HDACs whose knock-down phenotypically recapitulates chemical HDAC inhibition, we individually depleted class I, II, and IV HDACs by small interfering RNA (siRNA) and analyzed the changes in Golgi area and viability relative to nontargeting control siRNAs (Figure 3B and Supplemental Figure S2E). The highest level of Golgi dispersal was observed following HDAC1 knockdown. Loss of HDAC9 induced a level of Golgi structure reorganization similar to that of HDAC1 knockdown. This finding is surprising, since the chemical inhibition profiles of the HDAC inhibitors in our assays did not suggest an obvious implication of HDAC9. Knockdown of HDAC3 caused a small yet significant decrease in Golgi area compared with control, a phenotype opposite to the one observed with pharmacological inhibition of HDACs. siRNA-mediated depletion of HDAC4, HDAC5, and HDAC6 also led to Golgi complex disruption, albeit to a smaller degree than loss of HDAC1 or HDAC9. Evaluation of the knockdown efficiency of our siRNA pools demonstrated that the remaining fraction of protein or mRNA is significantly decreased compared with control siRNA treatment (Figure 3, C and D). Altogether, based on our findings using pharmacological reagents and genetic knockdown of HDACs, inhibition of HDAC1 appears to play a major role in the process of HDACi-mediated Golgi dispersal.

HDAC inhibition leads to increased protein trafficking rate but does not negatively affect glycosylation or Golgi dynamics

Previous reports have shown that Golgi fragmentation can occur during the execution phase of apoptosis (Lane *et al.*, 2002). Considering that knockdown of HDAC1 or HDAC2 both resulted in comparable loss of viability while displaying significantly different increases in Golgi area, these data suggested that the observed Golgi scattering is not due to induction of apoptosis (Figure 3B and Supplemental Figure S2E). In further support of this, neither cell survival nor the degree of Golgi dispersal caused by 72 h

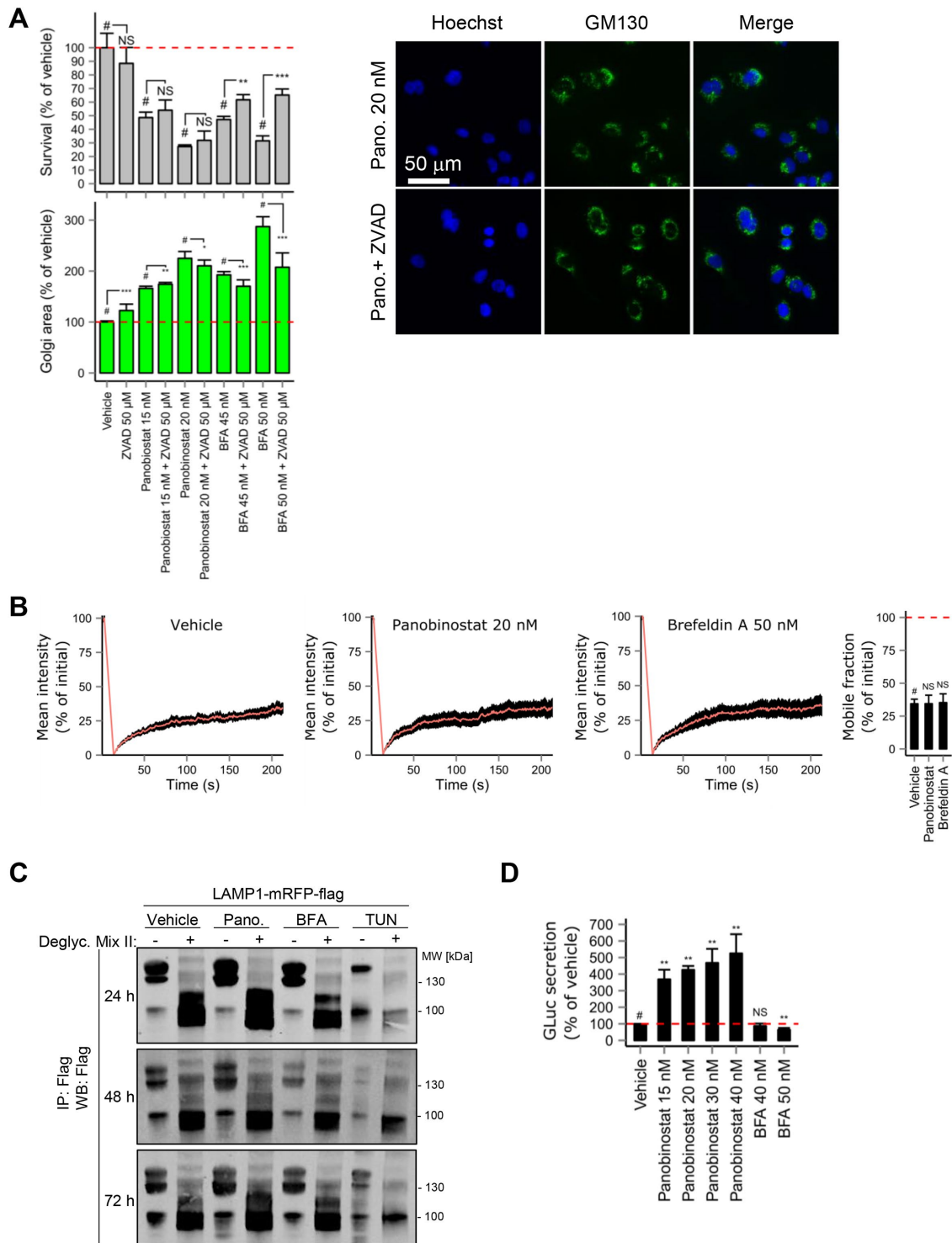


FIGURE 4: HDACi-mediated Golgi dispersal is not caused by apoptosis and does not alter lateral protein diffusion or glycosylation. (A) Quantification of Golgi area and survival ratios of A549 cells treated with Z-VAD-FMK alone or in combination with either Panobinostat or BFA for 72 h; representative images are shown on the right. (B) Fluorescence recovery after photobleaching performed with GalT-EGFP overexpressing A549 cells. Cells were treated for 72 h with vehicle, Panobinostat, or BFA before image acquisition. The average of seven measurements (orange line) plus SD (black error bars) normalized to initial intensity are shown. (C) Western blot analysis of glycosylation pattern of immunoprecipitated LAMP1-mRFP-flag, transiently expressed in HEK293T after treatment with either 20 nM Panobinostat, 50 nM BFA, or 500 nM Tunicamycin for the indicated amount of time. (D) Secretory activity of A549 cells transiently transfected with pCMV-GLuc for 48 h before treatment with vehicle, Panobinostat, or BFA for another 24 h. Representative data of two experiments are shown for A, C, and D and of one experiment for B. * $p < 0.05$ vs. #; ** $p < 0.01$ vs. #; *** $p < 0.001$ vs. #; see *Materials and Methods*.

protective effect on viability or Golgi shape on combination with VAD-FMK indicates that Golgi dispersal mediated by HDACi is not a result of apoptotic disassembly. To gain more insight into whether HDACi-induced Golgi structural changes impact lateral diffusion and mobility of proteins, we used fluorescence recovery after photobleaching (FRAP) of A549 cells that were stably transduced with the *trans*-Golgi marker GalT-EGFP (Ignashkova *et al.*, 2017) and treated with Panobinostat. The analysis shows that, relative to vehicle or 50 nM BFA treatment, no difference in the GFP recovery rate or the mobile fraction was observed at the end of monitoring indicating that proteins within and migrating to the Golgi apparatus are equally mobile in all of the conditions tested (Figure 4B). We further assessed Golgi functionality in response to HDACi by assessing the glycosylation pattern of LAMP1 (Terasawa *et al.*, 2016), which is subject to both N- and O-linked glycosylation (Wilke *et al.*, 2012; Li *et al.*, 2015). To this end, LAMP1-mRFP-flag was transiently overexpressed in HEK293T cells, which were then treated with vehicle, Panobinostat, BFA, or tunicamycin before Flag immunoprecipitation and subsequent treatment of half of the samples with a mixture of endo- and exoglycosidases that remove both N- and O-linked glycans. Relative to control condition treatment with the N-glycosylation inhibitor tunicamycin led to a collapse of glycosylated LAMP1 forms into one band. On incubation of tunicamycin-treated immunoprecipitates with the deglycosylation mix LAMP1 protein species were further modified, leading to the elimination of the higher-molecular-weight band, suggesting that removal of N- and O-linked sugars caused these shifts in electrophoretic mobility. On the other hand, neither Panobinostat nor BFA treatment caused discernible glycosylation alterations as judged by the band patterning and intensity on Western blot of exogenously expressed LAMP1 indicative of an absence of glycosylation defects following HDACi treatment (Figure 4C). Moreover, we interrogated the protein secretion ability of A549 cells transiently overexpressing Gaussia luciferase (GLuc). On BFA treatment, a decrease in secretory activity was observed as was also demonstrated previously (Ignashkova *et al.*, 2017). Surprisingly, in response to Panobinostat, the amount of GLuc secretion increased at all concentrations tested compared with vehicle treatment, indicating that protein transport along the secretory pathway is not blocked but rather enhanced on HDACi (Figure 4D). This effect could be related to previously reported findings on unstacking of Golgi cisternae following GRASP55/65 depletion, which resulted in enhanced protein trafficking (Xiang *et al.*, 2013; Bekier *et al.*, 2017).

Effect of HDAC inhibition on organelles

By analyzing the localization of the early Golgi protein GM130, we have already shown that HDACi leads to *cis*-Golgi dispersal (Figures 2B and 3, A and B). Next, we assessed the *trans*-Golgi subcompartment and *trans*-Golgi network (TGN) by IF microscopy using two additional Golgi markers. Staining with an antibody against endogenous TGN46, or stable expression of GalT-EGFP (Ignashkova *et al.*, 2017) revealed that in both cases Panobinostat treatment induced dispersal of the late Golgi comparable to GM130 IF (Supplemental Figure S3, A and B). Similarly, the staining pattern of ER-Golgi intermediate compartment (ERGIC) ERGIC-53, which marks the ERGIC, an organelle derived from the homotypic fusion of COPII vesicles and that lies between the ER and *cis*-Golgi (Hauri *et al.*, 2000), suggested an expanded area on Panobinostat treatment leading to an increased cytoplasmic distribution (Supplemental Figure S3C). To see whether HDACi treatment alters ER morphology, Panobinostat- and vehicle-treated cells were stained for protein disulfide isomerase (PDI). Compared to vehicle treatment, an expanded reticular-

like pattern of PDI was apparent on treatment with Panobinostat, suggestive of a more elaborate ER network, which could be due to ER stress induction (Supplemental Figure S4A). Interestingly, in our original phenotypic screen, several HDACis did not cause induction of another ER stress-responsive protein, the molecular chaperone GRP78, however, Panobinostat was not included in this analysis (Figure 2D). Taken together, from the ER to the *trans*-Golgi, all analyzed compartments displayed increases in their quantified area, which might support enhanced protein secretion (Figure 4D). Moreover, by immunostaining we further investigated the expression and localization of early endosomes using the EEA1 marker (Liberali *et al.*, 2014). Although not as apparent by visual inspection, automated image-based quantification of EEA1 suggests an enhanced area covered by early endosomes on HDACi and BFA treatment (Supplemental Figure S4B). Immunocytochemical labeling of actin filaments using phalloidin furthermore showed no differences in cell morphology and size of Panobinostat vs. vehicle- or BFA-treated cells (Supplemental Figure S4B). These data suggest that HDACi-mediated Golgi shape alterations are not due to indirect effects on the actin cytoskeleton. Last, incubation of A549 cells with Mitotracker Orange dye in the absence or presence of HDACi treatment did not noticeably change mitochondria mean signal intensity and only slightly increased quantified Mitotracker area, potentially suggesting that there is no apparent impact of Panobinostat on mitochondrial membrane potential in the surviving cells (Supplemental Figure S4C).

Combinatorial inhibition of HDACs and bromodomain containing proteins leads to enhanced Golgi dispersal and increased loss of viability

We have shown above that either chemical inhibition or genetic depletion of HDACs, which are also referred to as erasers of acetylated lysines, leads to Golgi morphology perturbation. We next asked whether inhibition of the readers of this epigenetic modification, the bromodomain containing proteins (BCPs) that act as principal acetylation recognition proteins, is similarly associated with changes in Golgi shape and/or could alter the observed Golgi phenotype in response to HDACis. To prevent the binding to acetylated lysine residues of the most studied family of proteins among the BCPs, we made use of the small molecule (+)-JQ1, which inhibits the bromodomain and extraterminal domain family (BET) of proteins (Ferri *et al.*, 2015). (+)-JQ1 has shown promising *in vitro* and *in vivo* anti-cancer effects and has a specific inhibitory profile for BETs (Filippakopoulos *et al.*, 2010; Dittmann *et al.*, 2014). Whereas (+)-JQ1 treatment on its own did not show noticeable effects on Golgi area and survival of A549 cells, the combination of (+)-JQ1 with the pan-HDAC inhibitor Panobinostat led to an enhancement of the HDACi-induced Golgi dispersal of A549 cells (Figure 5, A–E) and resulted in a decrease in cell survival compared with cells treated with Panobinostat alone (Figure 5C). Similar results were obtained when we combined Givinostat or Entinostat with (+)-JQ1. In both cases, the addition of (+)-JQ1 resulted in a further increase in Golgi area compared with single HDACi treatment (Supplemental Figure S5, A and B), coinciding with a significant decrease in viability (Supplemental Figure S5, C and D). These findings suggest that (+)-JQ1 can function as a modulator of Golgi morphology. We therefore decided to evaluate its properties also in combination with the Golgi disruptor BFA. Surprisingly, cotreatment of BFA and (+)-JQ1 significantly reduced BFA-induced Golgi fragmentation (Figure 5, B and E), while increasing the surviving fraction of the cells (Figure 5D). It was previously demonstrated that HDACs play a role in the DNA damage response (DDR) to

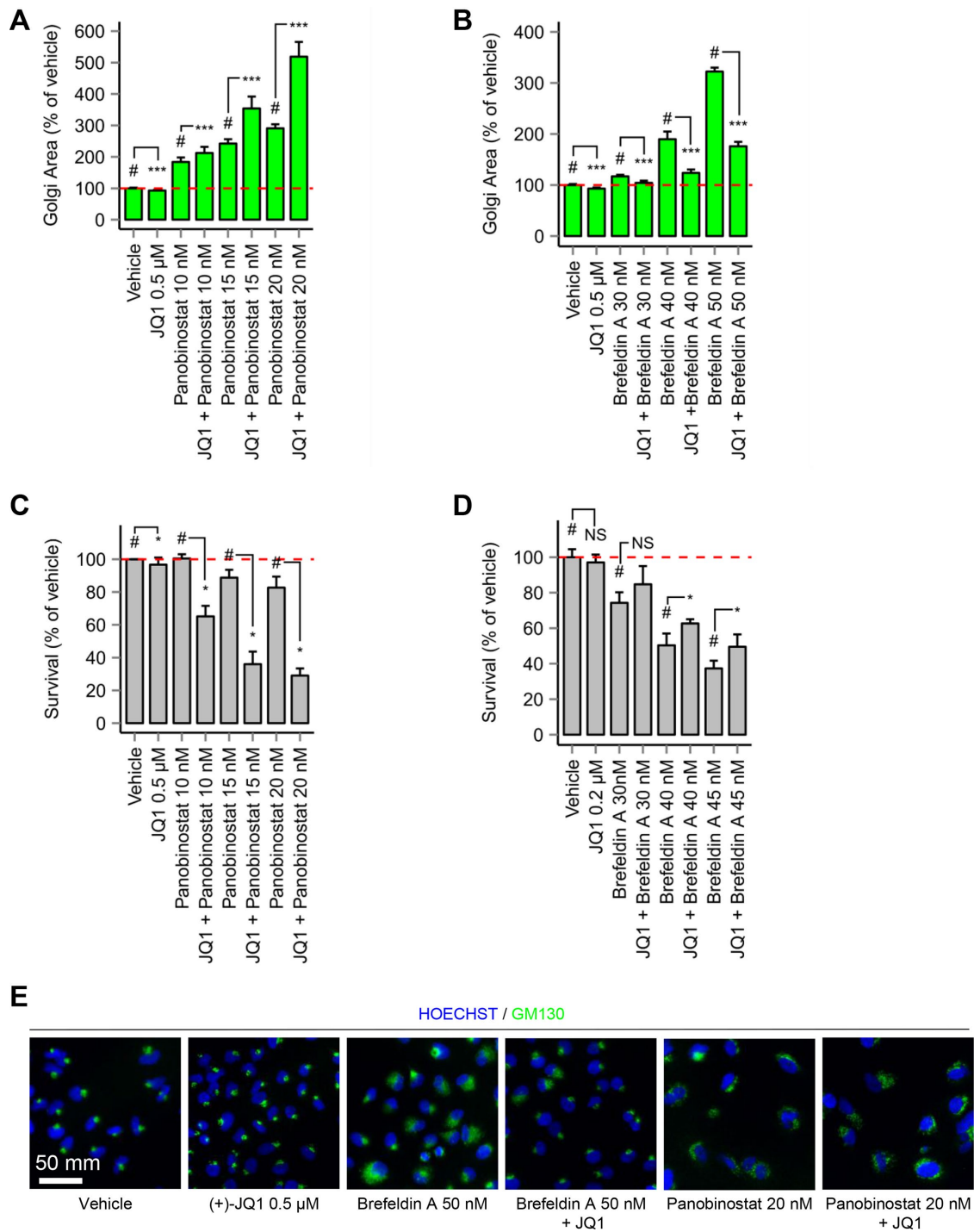


FIGURE 5: Inhibition of the bromodomain and extraterminal domain (BET) family of proteins using (+)-JQ1 enhances HDACi-induced Golgi dispersal while alleviating BFA-mediated Golgi scattering. (A) Quantification of Golgi area of A549 cells treated with (+)-JQ1 alone or in combination with Panobinostat for 72 h. (B) Quantification of Golgi area of A549 cells treated with (+)-JQ1 alone or in combination with BFA for 72 h. (C) Survival ratios of A549 cells treated for 72 h with (+)-JQ1 alone or in combination with Panobinostat were calculated by dividing the fluorescence values of compound-treated cells by fluorescence values of vehicle-treated cells using the CellTiter-Blue assay. (D) Survival ratios of A549 cells treated with (+)-JQ1 alone or in combination with BFA for 72 h. (E) Representative images of cells treated with single compounds or in combination (as indicated) are shown. * $p < 0.05$ vs. #; *** $p < 0.001$ vs. #; see *Materials and Methods*.

support nonhomologous end joining, and several HDACis were shown to cause increased γ H2AX levels, chromatin markers of double-strand breaks presumably due to unresolved DNA damage in

these cells (Tjeertes *et al.*, 2009; Miller *et al.*, 2010). To evaluate whether BCP inhibition influences this response, A549 cells were treated with (+)-JQ1, Panobinostat, or a combination thereof. The

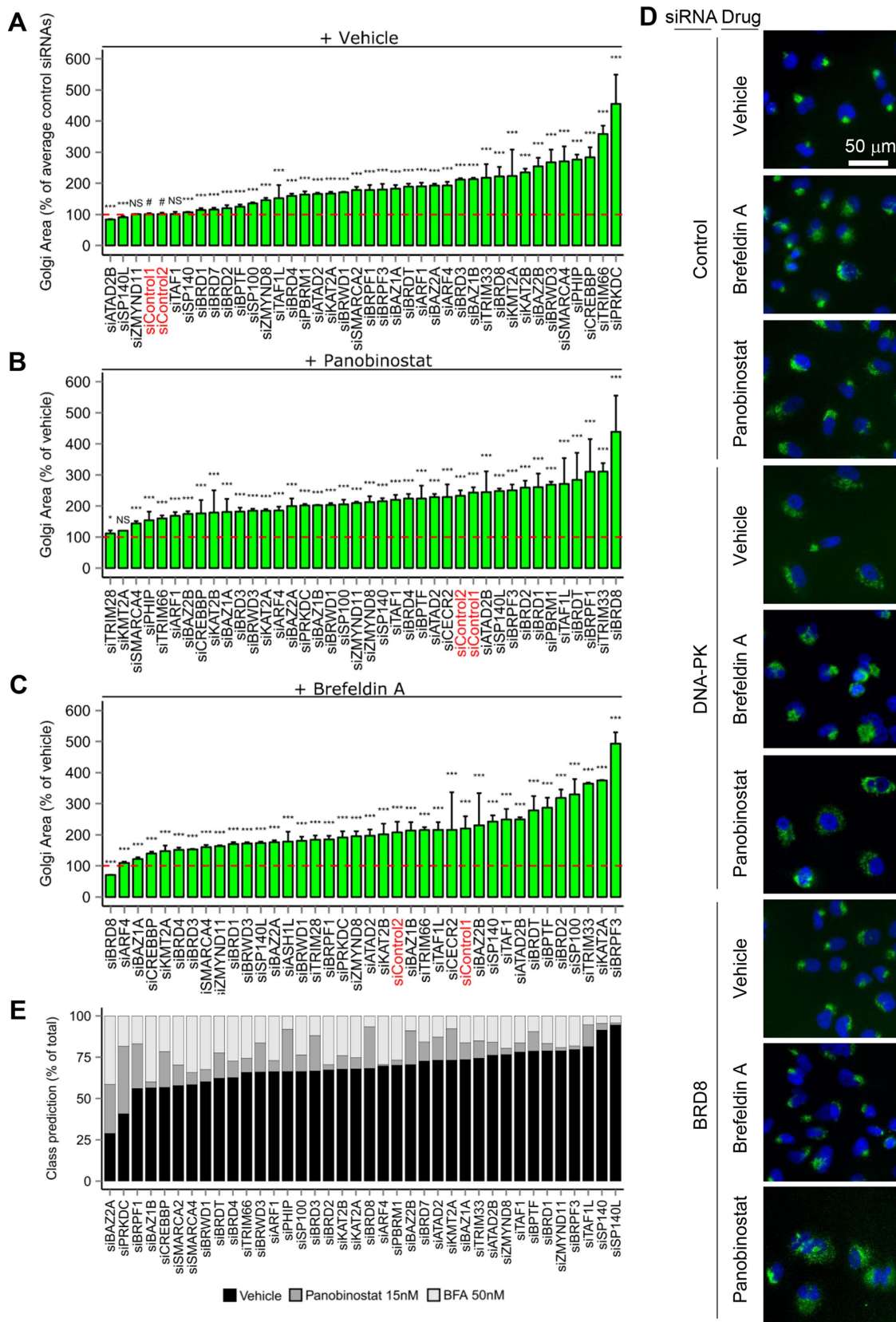


FIGURE 6: Knockdown of 43 bromodomain containing proteins identifies BRD8 as a potential mediator of BFA- and HDACi-induced Golgi dispersal. Based on the enhancement and mitigation of Golgi dispersal on combination of (+)-JQ1 and HDACi or BFA, respectively, systematic knockdown of individual BCPs was performed in A549 cells. Cells were transfected and incubated with siRNA for 48 h before treatment with either 50 nM BFA or 15 nM Panobinostat for 72 h. Cells were fixed, stained, and imaged for Golgi area measurements. (A) Quantification of Golgi area following

results presented in Supplemental Figure S5E demonstrate that (+)-JQ1 enhances γ H2AX levels in the presence of Panobinostat, which is indicative of elevated levels of DNA damage on cotreatment.

BFA is known to target certain ADP-ribosylation factor (ARF)–guanine nucleotide exchange factor complexes (Peyroche *et al.*, 1999), and alterations in the expression levels of different ARFs have been shown to selectively induce resistance or sensitivity to BFA. Knockdown of ARF1 induces sensitivity, while knockdown of ARF4 leads to BFA resistance (Reiling *et al.*, 2013; Ignashkova *et al.*, 2017). Even though BFA and HDACi treatments resulted in seemingly similar Golgi dispersal phenotypes, they appear to not follow identical mechanisms of action, since loss of ARF levels induced cellular sensitivity (shARF1) or resistance (shARF4) to BFA but did not change the cellular response to HDACi treatment (Supplemental Figure S6).

On the basis of the data presented so far, indicating a correlation of total acetylated histone levels induced by HDACi and the extent of Golgi dispersal (Figure 3A and Supplemental Figure S2, B and C) as well as the long treatment duration necessary to observe this phenotype (Supplemental Figure S2D), we hypothesized that these Golgi shape alterations may be transcriptionally mediated. Hence, we evaluated the effects of the transcription inhibitors α -Amanitin and Triptolide alone or in combination with Panobinostat on Golgi structure (Bensaude, 2011). Single α -Amanitin treatment caused a minor Golgi disruption (Supplemental Figure S7A). Remarkably, this response was even more pronounced with Triptolide, which led to significant Golgi dispersal by itself, and no additive effects were observed when it was combined with Panobinostat (Supplemental Figure S7B). The lack of cumulative effects suggests a shared mode of action between the HDACis and Triptolide, which could be due to similar transcriptional regulation of one or more genes whose products are involved in maintenance of Golgi structure in response to both compound classes. Further underscoring the importance of transcriptional regulation for Golgi structure maintenance might be the fact that the cyclin-dependent kinase/transcription inhibitor Flavopiridol, one of our phenotypic screening hits, also caused Golgi dispersal (Figure 2D). In the future, it will be of interest to identify the key genes regulated either at the transcriptional or posttranscriptional level that mediate the Golgi-dispersing effects of HDACis.

Knockdown of BRD8 mimics the effect of (+)-JQ1 in combination with either Panobinostat or Brefeldin A

The finding that the BET inhibitor (+)-JQ1 was able to modulate the Golgi morphology phenotype induced by HDAC inhibition or BFA treatment (Figure 5) prompted us to investigate which BCPs might mediate this effect. We thus assembled an siRNA library containing nontargeting controls, and siRNA pools targeting all known 42 BCPs (Fujisawa and Filippakopoulos, 2017) as well as ARF1 and ARF4 as positive controls for sensitivity and resistance to BFA, respectively. In addition, an siRNA pool targeting DNA-PK was included in our small-scale screen, because this protein kinase contains a bromodomain-like module, which specifically recognizes H2AX acetyl-lysine 5, in

turn regulating Ser139-H2AX phosphorylation (γ H2AX) by DNA-PK. Moreover, (+)-JQ1 can directly bind the BRD domain of DNA-PK, leading to the inhibition of its enzymatic activity (Wang *et al.*, 2015). We then assessed Golgi morphology changes in response to individual knockdown as well as in combination with Panobinostat or BFA. Depletion of several BCPs significantly decreased cell viability and/or increased the Golgi area, even without the addition of HDACi or BFA (Figure 6A and Supplemental Figure S8A). To exclude cell-death-related effects on Golgi morphology as a consequence of knockdown of some of the BCPs, we considered only those siRNA pools that had more than 150 surviving cells per well remaining. This yielded a list of 36 BCPs plus the two ARF isoforms that significantly altered the extent of Golgi spreading induced by BFA or Panobinostat (Figure 6, A–C, and Supplemental Figure S8B). The depletion of ARF4 protected the cells from BFA-induced Golgi dispersal as described previously (Reiling *et al.*, 2013). Remarkably, knockdown of BRD8 (Supplemental Figure S8C) showed an inverse phenotype when combined with either of the two Golgi disruptors, that is, loss of BRD8 enhanced the Golgi area increase caused by Panobinostat alone (Figure 6, B and D), while it completely prevented BFA-induced Golgi fragmentation (Figure 6, C and D). These results mimic our earlier results using (+)-JQ1. However, BRD8 was not reported thus far to be a direct (+)-JQ1 target. This suggests that Golgi morphology alterations in response to the combination of HDACi or BFA and (+)-JQ1 are linked to BRD8 inhibition. BRD8 expression has previously been shown to be down-regulated on pan-HDAC inhibition (Trichostatin A and Vorinostat) (Mackmull *et al.*, 2015). In this study, we corroborated these results by extending them to other HDACis (Panobinostat and Entinostat) (Supplemental Figure S8D). If loss of any individual BCP closely mimics the phenotype observed with BFA or Panobinostat treatment of wild-type cells, then this BCP might be involved in the signal transduction cascade triggered by the compounds. To further identify crucial contributors to the phenotypes observed with BFA or Panobinostat treatment, a machine-learning approach to classify the individual BCP knockdown without treatment was utilized. We trained a random forest algorithm using the data obtained for the nontargeting siRNA pools treated with vehicle, 50 nM BFA, or 15 nM Panobinostat to define the classifiers “vehicle,” “BFA,” or “Panobinostat.” We then applied the trained classifier on the data obtained for each vehicle-treated BCP knockdown to quantify which proportion of the cells derived from each knockdown corresponds to which predicted treatment class. This approach led to most of the cells being classified as “vehicle,” with the remaining fraction classified as either “BFA” or “Panobinostat,” the distribution of which determined whether the observed phenotype mostly resembled BFA or Panobinostat treatment (Figure 6E). As expected, loss of ARF1 led to a substantial fraction of cells to be classified as “BFA,” a result that is in line with published data describing ARF1 as a major mediator of the effects of BFA (Reiling *et al.*, 2013). Knockdown of BRD8 caused a large fraction of cells to be classified as “Panobinostat,” suggesting that BRD8 is involved in

siRNA-mediated knockdown normalized to the Golgi area of the control siRNA pools. (B) Quantification of Golgi area in response to individual gene knockdown and treated with 15 nM Panobinostat normalized to its own Golgi area under vehicle treatment conditions. (C) Quantification of Golgi area following individual knockdown treated with 50 nM BFA normalized to vehicle treatment of the same gene knockdown. (D) Representative images of selected knockdowns alone or with the indicated compound treatments are shown. (E) Assignment of individual phenotype classifiers (vehicle, BFA, or Panobinostat like) to (vehicle) knockdown cells using a machine-learning approach. The classifiers were obtained by training a random forest algorithm using images of cells transfected with nontargeting control siRNAs and treated with the corresponding small molecules. * $p < 0.05$ vs. # or control-siRNA; *** $p < 0.001$ vs. # or control-siRNA; see *Materials and Methods*.

the process of HDACi-mediated Golgi dispersal. Surprisingly, of all genes tested, knockdown of PRKDC (Supplemental Figure S8B), encoding the catalytic subunit of the DNA damage-repair protein DNA-dependent protein kinase (DNA-PK), caused the greatest extent of Golgi dispersal (Figure 6, A–D). Among all knockdowns, loss of DNA-PK was responsible for the highest fraction of cells to be classified as “Panobinostat,” suggesting that DNA-PK is critically involved in the process of HDACi-mediated Golgi dispersal (Figure 6E). It was recently reported that DNA damage inducers including doxorubicin, camptothecin, or ionizing radiation trigger Golgi disruption via DNA-PK-mediated GOLPH3 phosphorylation, the latter of which is a *trans*-Golgi-localized oncoprotein (Farber-Katz *et al.*, 2014). We therefore tested whether both factors are also involved in Golgi dispersal induced by HDACi treatment, which was evaluated in parallel to doxorubicin treatment. Relative to A549 cells treated with a control siRNA pool, knockdown of DNA-PK or GOLPH3 significantly increased Golgi area in the absence of compound treatment when markers for the *cis*-Golgi (GM130) or TGN (TGN46) were quantified by IF staining (Supplemental Figure S9). Interestingly, compared with control knockdown cells depletion of DNA-PK or GOLPH3 both prevented a further Golgi area increase induced by Panobinostat or doxorubicin as assessed by TGN46 staining (Supplemental Figures S9, A–D, and S11), a phenotype that was not as consistently observed using the GM130 Golgi marker although GOLPH3 knockdown also significantly protected from Panobinostat-induced *cis*-Golgi breakdown. Similar phenotypes albeit less pronounced were also observed in HeLa cells (Supplemental Figures S10 and S11). These observations suggest that GOLPH3 and DNA-PK play important roles in HDACi-mediated dispersal predominantly of the *trans*-Golgi/TGN. The results are consistent with previous findings demonstrating that GOLPH3 localizes to the *trans*-Golgi and that its knockdown phenotypically mostly affected *trans*-Golgi cisternae (Dippold *et al.*, 2009).

We further complemented our genetic knockdown analysis using pharmacological DNA-PK inhibition in the context of HDACi-induced Golgi dispersal. To this end, A549 cells were cotreated with the DNA-PK inhibitor NU7441 and Givinostat. Reminiscent of cells simultaneously treated with (+)-JQ1 and HDACis, NU7441 in combination with HDACi treatment led to a moderate enhancement of Golgi scattering (Supplemental Figure S12A). The extent of total levels of phosphorylated H2AX on DNA-PK inhibitor plus Givinostat cotreatment was also increased compared with Givinostat alone but less than the combination of this HDACi and (+)-JQ1 (Supplemental Figure S12B). We also tested KU55933, an inhibitor of the DDR kinase ATM, which can also phosphorylate H2AX (Burma *et al.*, 2001). In line with the results obtained with DNA-PK inhibition, ATM blockade slightly increased Golgi area and enhanced Golgi dispersal in combination with Givinostat (Supplemental Figure S12C). Confirming previous findings (Farber-Katz *et al.*, 2014) and underscoring the specificity of the observed phenotypes following HDACi, opposite effects (i.e., Golgi compaction) were observed after a combination of doxorubicin treatment and ATM or DNA-PK inhibition (Supplemental Figure S12D). Altogether, our results suggest that readers of acetylated lysines such as BRD8 and DNA-PK, previously recognized to be critically involved in DDR signaling (Gong *et al.*, 2016), are likely also involved in the process of HDACi-induced Golgi disintegration.

(+)-JQ1 and HDACi synergistically disperse the Golgi and reduce viability in a panel of cancer cell lines

We have shown that the simultaneous treatment of pan-HDACi and BETi leads to increased Golgi dispersal and associated loss of viability in the non-small cell lung adenocarcinoma cell line A549

compared with either single treatment (Figure 5, A, C, and E). This result prompted us to investigate other cancer cell line models. We therefore tested the combination of Panobinostat with (+)-JQ1 also in U251 (glioblastoma astrocytoma), PANC1 (pancreatic ductal adenocarcinoma), MDA-MB-231 (breast adenocarcinoma), and DU145 (prostate carcinoma) cells. Strikingly, a similar phenotypic pattern as with A549 cells was observed. U251 (Figure 7A), PANC1 (Figure 7B), MDA-MB-231 (Figure 7C), and DU145 (Figure 7D) cells displayed sensitization toward Panobinostat when combined with (+)-JQ1 as well as a higher degree of Golgi dispersal. We also observed that (+)-JQ1 alone lead to a significant increase in the proliferation of PANC1 cells, whereas the combination with Panobinostat induced synergistic loss of viability. Some studies already demonstrated the efficacy of the combination of Panobinostat and (+)-JQ1 for overcoming cellular resistance to certain kinase inhibitors (Fiskus *et al.*, 2014; Sun *et al.*, 2015) or showed increased cell death induction through decreased MYC expression (Mazur *et al.*, 2015; Shahbazi *et al.*, 2016). Our data might complement the aforementioned studies by suggesting that (+)-JQ1 facilitates the loss of integrity of the Golgi apparatus mediated by HDACi. This could be another reason why cells cotreated with BETi plus HDACi display synergistic lethality.

DISCUSSION

In this study, we have identified HDAC inhibitors and several DNA damage inducers as novel Golgi-disrupting compounds by two different approaches, namely 1) by gene expression profiling and comparative analysis with classical inducers of Golgi fragmentation (BFA, GCA, monensin) and 2) by phenotypic image-based high-content screening. Our results show that similarity in gene expression profiles in response to drug treatment can serve as an indicator for the manifestation of comparable phenotypic changes, validating once more the hypothesis that compounds with similar gene expression profiles are likely to share a related mechanism of action (Scherf *et al.*, 2000; Lamb, 2007; Hu and Agarwal, 2009; Iorio *et al.*, 2009, 2010). Ultrastructural analysis of the Golgi apparatus of HDACi-treated cells showed an accumulation of dilated and disorganized Golgi elements likely representing expanded cisternae, tubules, and associated vesicles (Supplemental Figure S2A). Several of the compounds identified as Golgi disruptors, such as Pracinostat (SB939) (Manal *et al.*, 2016), Panobinostat (Laubach *et al.*, 2015; Nervi *et al.*, 2015; Manal *et al.*, 2016), cisplatin (Kelland, 2007), 5-FU (Lee *et al.*, 2016), irinotecan (Wagner, 2015), teniposide (Kamal *et al.*, 2015), or etoposide/VP-16 (Yan *et al.*, 2016) are of high clinical relevance in the field of anti-cancer therapy, and it is intriguing to hypothesize that the effect on the Golgi contributes to their therapeutic potential. Remarkably, all of the HDACis used in this study led to comparable levels of Golgi dispersal, with the exception of Tubastatin A, an HDAC6-specific inhibitor. Reminiscent of Golgi complex perturbations caused by DNA damage inducers (Farber-Katz *et al.*, 2014), HDACi-induced Golgi dispersal is independent of apoptosis (Figure 4A), suggesting that Golgi structural rearrangements occur upstream of caspase activation, which then could either elicit adaptive or prodeath signal responses depending on the severity of the stress. Entinostat, which is more selective toward HDAC1 and HDAC3 (Hu *et al.*, 2003; Hess-Stump *et al.*, 2007; Bieliauskas and Pflum, 2008; Khan *et al.*, 2008), also induced Golgi dispersal, suggesting an important role for HDAC1 and/or HDAC3 in this process. Knockdown experiments confirmed the importance of HDAC1 for normal Golgi organization since loss of HDAC1 led to a dramatic increase in Golgi area akin to our observations using chemical HDAC inhibition. On

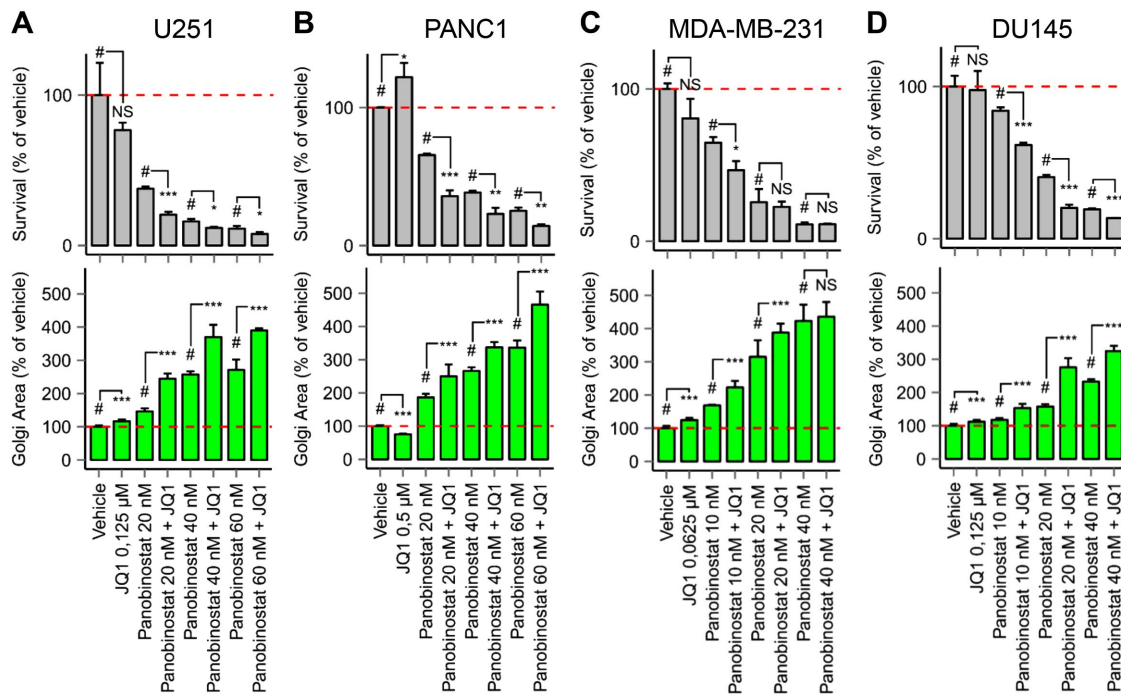


FIGURE 7: (+)-JQ1 and HDACi synergistically disperse the Golgi and reduce viability in a panel of cancer cell lines. The combination of Panobinostat and (+)-JQ1 was tested in a panel of cancer cell lines to evaluate the effects on Golgi morphology and viability (see also Figure 5). (A–D) Quantification of Golgi area and nuclei count of the indicated cell lines treated with (+)-JQ1 alone or in combination with Panobinostat for 72 h. Survival ratios of A549 cells treated with (+)-JQ1 alone or in combination with Panobinostat for 72 h were derived from nuclei counts of immunofluorescence experiments by dividing the number of nuclei present at the end of drug treatment by the number of nuclei present in the absence of drug treatment. Results from one representative example of two independent experiments are shown: * $p < 0.05$ vs. #; ** $p < 0.01$ vs. #; *** $p < 0.001$ vs. #; #; see *Materials and Methods*.

the other hand, compared with Entinostat treatment siRNA-mediated knockdown of HDAC3 led to the opposite phenotype, that is, a marginal but significant compaction of the Golgi, thereby further emphasizing the critical contribution of HDAC1 but not HDAC3 to Golgi dispersal following Entinostat treatment. Interestingly, rivaling the effect of HDAC1 (class I HDAC) knockdown, loss of HDAC9 also led to a large increase in Golgi spreading, indicating a critical role also for this class II HDAC in modulating Golgi shape. In addition to the putative HDACs leading to Golgi dispersal, we also present evidence suggesting that the phenotypic alterations are brought about by transcriptional changes, because 1) several transcription inhibitors tested cause Golgi disruption, 2) the combination of HDACi with Triptolide did not result in further enhancement of Golgi disintegration, and 3) significant HDACi-induced effects on Golgi morphology can only be observed after several hours of treatment but not in response to short-term incubation. We also show that HDACi-mediated Golgi dispersal affects both *cis*- and *trans*-Golgi/TGN compartments in addition to the ERGIC and also increased PDI ER marker staining and early endosomal area. On the other hand, no obvious alterations to the actin cytoskeleton were detected. It appears that in our experimental setup Panobinostat treatment has no negative impact on protein glycosylation but causes enhanced trafficking of a reporter protein through the Golgi, suggesting that normal transport of certain proteins or lipids might be altered following HDACi. Moreover, FRAP experiments revealed that lateral diffusion within the Golgi is unchanged compared with vehicle treatment.

Importantly, the combination of HDACis with (+)-JQ1, an inhibitor of the BET family of BCPs, enhanced HDACi-mediated Golgi dispersal and was associated with a substantial decrease in viability. The strong attenuation of viability on combination of (+)-JQ1 and Panobinostat or SAHA in human acute myelogenous leukemia, neuroblastoma, or pancreatic ductal adenocarcinoma has recently been described (Fiskus *et al.*, 2014; Mazur *et al.*, 2015; Shahbazi *et al.*, 2016) and involves the HDACi-induced down-regulation of c-Myc or N-Myc, respectively. We complement these observations with a new proposal: the cells might be more susceptible to the combination treatment because of a synergistic effect on loss of Golgi integrity. Enhanced Golgi dispersal associated with lower survival in response to HDACi/(+)-JQ1 treatment was found in several cancer types (lung, pancreas, prostate, breast, glioblastoma), which is suggestive of a more general phenomenon. In contrast to Panobinostat, the combination of which with (+)-JQ1 resulted in enhanced Golgi disruption, the co-treatment of BFA, and (+)-JQ1 suppressed Golgi fragmentation typically mediated by BFA alone. Indeed, the phenotype induced by simultaneous exposure to BFA and (+)-JQ1 is strictly opposite compared with coincubation of cells with Panobinostat and (+)-JQ1. These data suggest that the same factors are involved in the mode of alterations to Golgi structure triggered by both drugs but leading to differing phenotypes when combined with (+)-JQ1. Additionally, we observed that pharmacological inhibition of DNA-PK also enhanced the dispersal mediated by HDACi, similarly to (+)-JQ1 but less severe (Supplemental Figure S12A). Furthermore, DNA-PK knockdown cells displayed a fragmented

Golgi phenotype that our machine-learning approach classified as Panobinostat-like. DNA-PK and GOLPH3 were previously implicated in DNA damage-induced Golgi dispersal (Farber-Katz *et al.*, 2014). We found that in response to HDACi, DNA-PK and GOLPH3 exert a pronounced effect on the late Golgi, because knockdown of either gene prevented further Panobinostat-induced *trans*-Golgi/TGN dispersal. These data suggest that DNA-PK is also mechanistically involved in HDACi-mediated Golgi morphology alterations. DNA-PK contains a noncanonical bromodomain involved in DNA damage signaling that can be targeted by (+)-JQ1 (Wang *et al.*, 2015). Indeed, inhibition of either the catalytic site or the bromodomain of DNA-PK resulted in an aggravation of the HDACi-mediated Golgi dispersal paralleled by increased γ -H2AX levels (Supplemental Figure S12B). To assess whether BCPs, which recognize acetylated lysine residues in histone and nonhistone proteins, mediate Golgi dispersal downstream of HDACi, an image-based phenotypic small-scale siRNA screen was performed. The systematic knockdown of BCPs revealed that, of all BCPs tested, BRD8 depletion mimics most closely the effects of (+)-JQ1, both in the context of Panobinostat- and BFA-mediated Golgi dispersal. Loss of BRD8 led to an enhancement of Panobinostat-mediated Golgi disruption while attenuating the fragmentation induced by BFA. Taken together, these data suggest 1) that BRD8 is a putative target of (+)-JQ1 and 2) that BRD8 is responsible for the changes in Golgi dispersal triggered by the BET inhibitor in combination with BFA or HDACi. Despite the fact that the binding of (+)-JQ1 to BRD8 has not been reported thus far (Filippakopoulos *et al.*, 2010), the amino acid similarity between the two (+)-JQ1-binding bromodomains of BRD4 and the first bromodomain of BRD8 are between 32 and 45% (Supplemental Figure S13A), which may be sufficient for (+)-JQ1 binding. Indeed, all bromodomains of the BET family BCPs display high similarity to the first bromodomain of BRD8 (Supplemental Figure S13B). On the basis of these similarities and the results of this study, we hypothesize that BRD8 is a putative new target of (+)-JQ1. Interestingly, the phenotypic effects obtained through the use of (+)-JQ1 or RNAi-induced BRD8 knockdown seem to differ as the former causes a slight Golgi compaction (Figure 5, A and B) and the latter Golgi dispersal (Figure 6A). It could be that the scaffolding functions of BRD8 may still be functional on BET inhibition using (+)-JQ1 when the dispersal is not occurring, whereas upon knockdown, this function becomes rate-limiting, and loss of normal Golgi structure ensues. Another mutually nonexclusive possibility is that (+)-JQ1 targets multiple BCPs (Filippakopoulos *et al.*, 2010), the combined inhibition of which results in a somewhat different phenotype than single BRD8 knockdown. Most importantly, the HDACi-mediated down-regulation of BRD8 (Supplemental Figure S8D) could explain why we observe an enhancement of Panobinostat-mediated Golgi dispersal by BET inhibition or BRD8 knockdown: in a context of HDACi-induced transcriptional BRD8 down-regulation, the remaining fraction of BRD8 is inhibited by the BET inhibitor that exacerbates the Golgi disruption. In fact, BRD8 knockdown increases the fraction of cells classified as "Panobinostat-like"-treated cells despite the absence of the chemical (Figure 6E). This phenotypic similarity suggests a role for BRD8 in Panobinostat-mediated Golgi dispersal, especially in combination with (+)-JQ1.

The discovery of pan-HDACi-mediated Golgi dispersal might offer new therapeutic avenues for treating cancer. We show here that facilitating the loss of Golgi integrity with a BETi sensitizes cells to pan-HDACi in several different cancer types. Using this approach, a smaller dosage of pan-HDACi is needed to achieve the same effects of higher doses of pan-HDACi alone and could, consequently, decrease toxic side effects associated with current HDACi treatment

regimens. The prevention of negative side effects could substantially improve the quality of life of patients without sacrificing treatment efficacy.

MATERIALS AND METHODS

Cell culture and reagents

All cell lines described were grown in high-glucose DMEM (Life Technologies) with 10% heat-inactivated fetal bovine serum (FBS) in the presence of 100 U/ml penicillin and 100 μ g/l streptomycin (Life Technologies). Compounds were obtained from the following companies: brefeldin A (Sigma-Aldrich), golgicide A (Santa Cruz Biotechnology), monensin (Enzo Life Sciences), AG-1478 (Sigma), tunicamycin (Santa Cruz Biotechnology), thapsigargin (Santa Cruz Biotechnology), nocodazole (Santa Cruz Biotechnology), (+)-JQ1 (Cayman Chemical), CBP30 (TargetMol), doxorubicin (Sigma), etoposide (Sigma), teniposide (Santa Cruz Biotechnology), mitomycin-C (Santa Cruz Biotechnology), cisplatin (Santa Cruz Biotechnology), hydroxyurea (Sigma), 5-fluorouracil (Sigma), gemcitabine (Santa Cruz Biotechnology), irinotecan (Santa Cruz Biotechnology), bleomycin (Santa Cruz Biotechnology), NU7441 (Selleckchem), KU55933 (Sigma), Flavopiridol (Santa Cruz Biotechnology), phorbol 12-myristate 13-acetate (PMA; Santa Cruz Biotechnology), Panobinostat (Selleckchem), Tubastatin (Selleckchem), Entinostat (Santa Cruz Biotechnology), Pracinostat (Selleckchem), Givinostat (Selleckchem), Triptolide (Santa Cruz Biotechnology), α -Amanitin (Santa Cruz Biotechnology), and Z-VAD-FMK (Santa Cruz Biotechnology). For the genetic knockdown experiments using siRNA, the pools of four different siRNAs targeting the same gene were purchased from Dharmacon. For the high-content screen, an epigenetic library (Cayman Chemical; #11076), a custom-assembled kinase inhibitor library (Merck-proprietary compounds), and Mini Library (more information at www.merckgroup.com/en/research/open-innovation/biopharma-open-innovation-portal/biopharma-mini-library.html) were used. The latter two libraries were obtained from Merck KGaA. For most knockdown experiments siRNAs were used with the exception of Supplemental Figure S6, wherein lentiviral hairpins were used to knockdown ARF1 or ARF4. shRNAs with the following TRC hairpin IDs (Mission shRNAs, Sigma-Aldrich) were used:

shARF1#1: TRCN0000039874 shARF1#2: TRCN0000039876
shARF4#1: TRCN0000039876 shARF4#2: TRCN0000047938

siRNA transfection

Pools of four different siRNAs targeting the same gene were purchased from Dharmacon. All siRNA experiments to knockdown individual genes were performed as reverse transfections. DharmaFECT 1 Transfection Reagent (Dharmacon; #T-2001-01) was mixed with DharmaFECT Cell Culture Reagent (Dharmacon; #B004500100) to obtain a 1% solution. siRNAs were added to this mixture (25 nM final concentration) and incubated for 20 min at room temperature. The transfection mix was added to the corresponding well or dish. Cells were dispensed on top of the transfection mix at a concentration described in the corresponding experimental methods section.

Immunofluorescence

For immunofluorescence microscopy, 1500 cells were seeded per 96-well plate in 80 μ l media and treated as indicated. After incubation for the desired time under the treatment conditions specified for each experiment, cells were fixed using 4% paraformaldehyde (Electron Microscopy) for 20 min at room temperature. Wells were washed twice using phosphate-buffered saline (PBS) before permeabilization using 0.05% Triton X-100 (Amresco) in PBS for

20 min at room temperature. Afterward, wells were washed twice with PBS before adding the primary antibody against GM130 (1:100, sc-16268; Santa Cruz Biotechnology), TGN46 (1:2000; Bio-Rad), ERGIC-53 (1:100; Santa Cruz Biotechnology), EEA1 (1:500; Cell Signaling Technology), or PDI (1:500; Cell Signaling Technology) and were diluted in 5% normal donkey serum (NDS; Jackson Immune Research) in PBS. Samples were incubated overnight at 4°C. Samples were washed thrice with PBS before incubation with the appropriate secondary antibody; coupled to Alexa Fluor 488, 568, or 647 (1:2000; Life Technologies); combined with Hoechst (1:2500; Life Technologies; #33342) and/or Phalloidin (1:500; Life Technologies; #A12380); and diluted in 5% NDS in PBS for 1 h at room temperature. After staining, samples were washed four times with PBS. Images were acquired with an Olympus Biosystems IX81 wide-field inverted microscope (equipped with an electron-multiplying charge-coupled device [EM-CCD] Hamamatsu C9100-2 camera) at 20× magnification (UPLSAPO 20× air objective, aperture of 0.75). The acquisition was performed at room temperature using the software Olympus ScanR version 2.5.0. For the high-content screen performed using 96-well plates (Greiner Bio-One), 20 fields per well were acquired; for validation experiments, 16 fields were acquired per well. For mitochondria staining, cells were incubated with 100 nM of MitoTracker Orange CMTMRos (Invitrogen) at 37°C and 5% CO₂ for 1 h before fixing the cells and staining for other cellular compartments as described above.

Fluorescence recovery after photobleaching

For FRAP, 3500 A549 cells stably overexpressing GalT-EGFP (EGFP C-terminally fused to the 60 first amino acids of β -1,4-galactosyltransferase 1 [B4GALT1]) were plated in 300 μ l media in eight-well μ -slides (ibidi) and allowed to adhere overnight. The cells were then treated with indicated drug concentrations for 72 h. A Leica TCS SP5 confocal microscope was used to photobleach a fraction of the Golgi of seven different cells per condition tested as shown in previous studies (Picaud *et al.*, 2013). The objective used was an HCX Plan APO 40× oil immersion with a high-numerical-aperture (N.A. 1.3). At least 60% of the initial signal was depleted after photobleaching. The recovery of the fluorescence signal was monitored over 213 s after photobleaching. Cells were maintained at 37°C and 5% CO₂ during the entire acquisition procedure.

Deglycosylation assay

The amount of 500,000 HEK293T cells per condition were transiently transfected with LAMP1-mRFP-flag (0.5 μ g DNA with 1.5 μ l of TransIT-LT1 [Mirus]). Twenty-four hours after transfection, cells were treated with the indicated compounds and concentration for 24, 48, or 72 h before cells lysis and Flag immunoprecipitation. LAMP1-mRFP-flag was immunoprecipitated using anti-FLAG M2 Affinity Gel (Sigma-Aldrich). Afterward, samples were prepared using the Deglycosylation Mix II (#P6044S; New England Biolabs) according to the manufacturer's recommendation. After treatment with the deglycosylation mix II, samples were immunoblotted with the indicated antibody.

Gaussia luciferase secretion assay

The amount of 500,000 A549 cells were reverse-transfected with 0.5 μ g of pCMV-GLuc using 1.5 μ l of TransIT-LT1 (Mirus) in 10-cm dishes. Twenty-four hours after transfection, 5000 cells were plated in 100 μ l medium per well in 96-well plates. Twenty-four hours afterward, cells were treated for another 24 h with the indicated compounds, after which 50 μ l of culture supernatant was transferred to a white, opaque 96-well plate. Freshly prepared Gaussia luciferase

flash assay reagent (20 μ l; Pierce) was added, and the luminescence signal was read after 10 s of integration time using a Glomax Multi Detection plate reader (Promega). The level of secretory activity of cells was determined as a ratio calculated by normalizing all samples to the vehicle control after a background signal subtraction step.

Transmission electron microscopy

A549 cells were embedded in epoxy resin for ultrathin sectioning according to standard procedures: cells grown on punched Aklar slips were fixed in buffered aldehyde (2% formaldehyde, 2% glutaraldehyde, 2 mM MgCl₂ in 100 mM Na-phosphate, pH 7.2), and post-fixed in buffered 1% osmium tetroxide followed by en bloc staining in 1% uranylacetate/75% ethanol. Following dehydration in graded steps of ethanol, the adherent cells were flat-embedded in Epoxide (Glycidether, NMA, DDSA; Serva, Heidelberg, Germany). Ultrathin sections at nominal thickness of 60 nm and contrast-stained with lead-citrate and uranylacetate were analyzed using a Zeiss EM 910 at 120-kV electron microscope (Carl Zeiss), and micrographs were taken with image-plates, scanned at 30- μ m resolution (Ditabis micron).

Image processing and feature extraction

Images were processed and data analyzed using the KNIME Analytics Platform (Petri and Meister, 2013; Dietz and Berthold, 2016). Segmentation and feature extraction was performed similarly to previous work (Carpenter *et al.*, 2006; Held *et al.*, 2010). Briefly, nuclei were segmented using an Otsu thresholding method (Otsu, 1979). Then nuclei were extended to the border of the cell body using a Voronoi algorithm set to stop when the intensity dropped below a defined threshold. The vesicles composing the Golgi apparatus were identified with an Otsu global thresholding method (Otsu, 1979) combined with a Bersen local thresholding method (Chen and Leung, 2004). The structures identified in this manner were then mapped back to their corresponding cell using the predefined cellular masks.

Phenotypic classification

Classification of phenotypes was done within the KNIME Analytics Platform (Petri and Meister, 2013; Dietz and Berthold, 2016) using a random forest algorithm (Touw *et al.*, 2013; Hedberg-Buenz *et al.*, 2016). The cells transfected with nontargeting control siRNAs and treated with vehicle, 50 nM BFA, or 15 nM Panobinostat were used to train the model. Eighty percent of the training set was used to train the model and the remaining 20% used for cross-validation. This step was repeated five times with a new random split at each iteration. The model obtained was then used to classify the cells transfected with the siRNA pools targeting the genes of interest and left untreated to assign them to the classes "vehicle," "BFA," or "Panobinostat." The classification was also repeated 5 times before calculating the mean of each predicted class. Classes are expressed as a fraction of the total cell population for each individual knockdown.

Viability assays

For viability assays, cells were plated in 96-well plates (Greiner Bio One) and allowed to adhere overnight. After incubation for the desired time under the treatment conditions specified for each experiment, CellTiter-Blue viability stain (Promega) was used to quantify live cells. Fluorescent end product resorufin was measured using a Glomax Multi Detection plate reader (Promega), and all values were normalized to the appropriate vehicle control.

Western blotting

Immunoblotting experiments were performed using standard protocols. Cells were lysed in RIPA buffer containing protease and

phosphatase inhibitors (Roche Applied Science) and proteins were resolved by SDS-PAGE on 4–12% NuPAGE Novex gradient Bis-Tris gels (Thermo Fisher Scientific) and transferred to polyvinylidene difluoride (PVDF) membranes (Immobilon). Membranes were blocked in Licor Odyssey Blocking Buffer (LI-COR). Primary antibody incubation was performed in blocking buffer containing 0.1% Tween overnight at 4°C. Proteins were visualized using species-specific far-infrared dye-coupled secondary antibodies (LI-COR) on a LI-COR Odyssey Sa scanner using Image Studio software (LI-COR). The following primary antibodies were used: p84 (1:1000, GTX70220, Genetex), pan-Ac-Lys (1:5000, #9441; Cell Signaling), cleaved poly ADP-ribose polymerase (PARP; 1:750, #5625; Cell Signaling), pH2AX (1:1000, #9718; Cell Signaling), and β -actin (1:15,000, #3700; Cell Signaling).

Statistical methods

The significance of the compound enrichment in the top 50 hits of the connectivity map analysis was calculated by comparing the representation factor of the observed compound groups to that of randomly chosen compound groups from the total number of compounds in the analysis.

Statistical significance of immunofluorescence measurements was calculated using the entire cell populations of the three replicates within one representative experiment of three independent experiments. Significance was assessed using the independent groups *t* test by comparing samples of interest either to vehicle control or to #-labeled samples (**p* < 0.05 vs. vehicle or #; ***p* < 0.01 vs. vehicle or #; ****p* < 0.001 vs. vehicle or #). The data are displayed as mean and SD.

Survival ratios were determined either by the CellTiter-Blue assay described above or by nuclei counts obtained from immunofluorescence experiments. Significance was assessed using one-way analysis of variance by comparing samples either to vehicle control or to #-labeled samples (**p* < 0.05 vs. vehicle or #; ***p* < 0.01 vs. vehicle or #; ****p* < 0.001 vs. vehicle or #). The data are displayed as mean and SD of the three replicates within one representative experiment of three independent experiments.

Statistical significance for mRNA expression levels obtained by real-time quantitative reverse transcription PCR (qRT-PCR) were calculated by paired *t* test using the mean of three independent experiments comparing either to vehicle control or to control-siRNA transfected sample (**p* < 0.05 vs. vehicle or control-siRNA; ***p* < 0.01 vs. vehicle or control-siRNA; ****p* < 0.001 vs. vehicle or control-siRNA). The data are displayed as mean and SD of three independent experiments.

ACKNOWLEDGMENTS

We thank the BioMed X IMT team for the use of the epigenetic compound library and Merck KGaA for providing us with the kinase inhibitor library and the Mini Library. We also thank Holger Erfle, Manuel Gunkel, and Jürgen Reymann for their help with image acquisition of the high-content screen at BioQuant (Heidelberg) and their support with image processing. In addition, we thank Holger Lorenz (imaging facility at ZMBH, Heidelberg) for his assistance and helpful discussions and Roberto Zoncu (University of California at Berkeley) for providing us with the LAMP1-mRFP-flag cDNA (from rat) construct. We are also thankful to Karsten Richter and Michelle Neßling for the preparation of the cells for TEM and image acquisition at the Central Unit Electron Microscopy of the German Cancer Research Center (Heidelberg).

REFERENCES

- Atadja P (2009). Development of the pan-HDAC inhibitor panobinostat (LBH589): Successes and challenges. *Cancer Lett* 280, 233–241.
- Bailey H, Stenehjem DD, Sharma S (2015). Panobinostat for the treatment of multiple myeloma: the evidence to date. *J Blood Med* 6, 269–276.
- Bartling B, Hofmann H-S, Boettger T, Hansen G, Burdach S, Silber R-E, Simm A (2005). Comparative application of antibody and gene array for expression profiling in human squamous cell lung carcinoma. *Lung Cancer* 49, 145–154.
- Bekier ME 2nd, Wang L, Li J, Huang H, Tang D, Zhang X, Wang Y (2017). Knockout of the Golgi stacking proteins GRASP55 and GRASP65 impairs Golgi structure and function. *Mol Biol Cell* 28, 2833–2842.
- Bensaude O (2011). Inhibiting eukaryotic transcription: which compound to choose? How to evaluate its activity? *Transcription* 2, 103–108.
- Bieliauskas AV, Pflum MKH (2008). Isoform-selective histone deacetylase inhibitors. *Chem Soc Rev* 37, 1402.
- Burma S, Chen BP, Murphy M, Kurimasa A, Chen DJ (2001). ATM phosphorylates histone H2AX in response to DNA double-strand breaks. *J Biol Chem* 276, 42462–42467.
- Butler KV, Kalin J, Brochier C, Vistoli G, Langley B, Kozikowski A (2010). Rational design and simple chemistry yield a superior, neuroprotective HDAC6 inhibitor, tubastatin A. *J Am Chem Soc* 132, 10842–10846.
- Cancino J, Luini A (2013). Signaling circuits on the Golgi complex. *Traffic* 14, 121–134.
- Carpenter AE, Jones TR, Lamprecht MR, Clarke C, Kang IH, Friman O, Guertin DA, Chang JH, Lindquist RA, Moffat J, et al. (2006). CellProfiler: image analysis software for identifying and quantifying cell phenotypes. *Genome Biol* 7, R100.
- Chen S, Leung H (2004). Chaotic spread spectrum watermarking for remote sensing images. *J Electron Imaging* 13, 146–165.
- Chia J, Goh G, Racine V, Ng S, Kumar P, Bard F (2012). RNAi screening reveals a large signaling network controlling the Golgi apparatus in human cells. *Mol Syst Biol* 8, 629.
- Chiu VIK, Bivona T, Hach A, Sajous JB, Silletti J, Wiener H, Johnson RL, Cox AD, Philips MR (2002). Ras signalling on the endoplasmic reticulum and the Golgi. *Nat Cell Biol* 4, 343–350.
- Choudhary C, Kumar C, Gnäd F, Nielsen ML, Rehman M, Walther TC, Olsen JV, Mann M (2009). Lysine acetylation targets protein complexes and co-regulated major cellular functions. *Science* 325, 834–840.
- Dietz C, Berthold MR (2016). KNIME for open-source bioimage analysis: a tutorial. *Focus Bio-Image Inform* 219, 179–197.
- Dippold HC, Ng MM, Farber-Katz SE, Lee S-K, Kerr ML, Peterman MC, Sim R, Wiharto PA, Galbraith KA, Madhavarapu S, et al. (2009). GOLPH3 bridges phosphatidylinositol-4-phosphate and actomyosin to stretch and shape the Golgi to promote budding. *Cell* 139, 337–351.
- Dittmann A, Werner T, Chung CW, Savitski MM, Savitski MF, Grandi P, Hopf C, Lindon M, Neubauer G, Prinjha RK, et al. (2014). The commonly used PI3-kinase probe LY294002 is an inhibitor of BET bromodomains. *ACS Chem Biol* 9, 495–502.
- Ewig RA, Fornace AJ (1976). Single-strand scission and repair of DNA in mammalian cells by bleomycin. *Cancer Res* 36, 3834–3838.
- Falkenberg KJ, Johnstone RW (2014). Histone deacetylases and their inhibitors in cancer, neurological diseases and immune disorders. *Nat Rev Drug Discov* 13, 673–691.
- Farber-Katz SE, Dippold HC, Buschman MD, Peterman MC, Xing M, Noakes CJ, Tat J, Ng MM, Rahajeng J, Cowan DM, et al. (2014). DNA damage triggers Golgi dispersal via DNA-PK and GOLPH3. *Cell* 156, 413–427.
- Ferri E, Petosa C, McKenna CE (2015). Bromodomains: structure, function and pharmacology of inhibition. *Biochem Pharmacol* 106, 1–18.
- Filippakopoulos P, Qi J, Picaud S, Shen Y, Smith WB, Fedorov O, Morse EM, Keates T, Hickman TT, Felletar I, et al. (2010). Selective inhibition of BET bromodomains. *Nature* 468, 1067–1073.
- Fiskus W, Sharma S, Qi J, Shah B, Devaraj SGT, Leveque C, Portier B, Iyer S, Bradner JE, Bhalla KN (2014). BET protein antagonist JQ1 is synergistically lethal with FLT3 tyrosine kinase inhibitor (TKI) and overcomes resistance to FLT3-TKI in AML cells Expressing FLT-ITD. *Mol Cancer Ther* 13, 2315–2327.
- Fujisawa T, Filippakopoulos P (2017). Functions of bromodomain-containing proteins and their roles in homeostasis and cancer. *Nat Rev Mol Cell Biol* 18, 246–262.
- Fujiwara O, Yokota T, Ikehara (1988). Brefeldin A causes disassembly of the Golgi complex and accumulation of secretory proteins in the endoplasmic reticulum. *J Biol Chem* 263, 18545–18552.

- Gong F, Chiu LY, Miller KM (2016). Acetylation reader proteins: linking acetylation signaling to genome maintenance and cancer. *PLoS Genet* 12, e1006272.
- Grunstein M (1997). Histone acetylation in chromatin structure and transcription. *Nature* 389, 349–352.
- Halberg N, Sengelaub CA, Navrazhina K, Molina H, Uryu K, Tavazoie SF (2016). PITPNC1 recruits RAB1B to the Golgi network to drive malignant secretion. *Cancer Cell* 29, 339–353.
- Hauri HP, Kappeler F, Andersson H, Appenzeller C (2000). ERGIC-53 and traffic in the secretory pathway. *J Cell Sci* 113, 587–596.
- Hecht SM (2000). Bleomycin: new perspectives on the mechanism of action 1. *J Natur Prod* 63, 158–168.
- Hedberg-Buenz A, Christopher MA, Lewis CJ, Fernandes KA, Dutca LM, Wang K, Scheetz TE, Abramoff MD, Libby RT, Garvin MK, et al. (2016). Quantitative measurement of retinal ganglion cell populations via histology-based random forest classification. *Exp Eye Res* 146, 370–385.
- Held M, Schmitz MHA, Fischer B, Walter T, Neumann B, Olma MH, Peter M, Ellenberg J, Gerlich DW (2010). Cell cognition: time-resolved phenotype annotation in high-throughput live cell imaging. *Nat Methods* 7, 747–754.
- Hertel LW, Boder GB, Kroin JS, Rinzel SM, Poore GA, Todd GC, Grindey GB (1990). Evaluation of the antitumor activity of gemcitabine (2',2'-difluoro-2'-deoxycytidine). *Cancer Res* 50, 4417–4422.
- Hess-Stumpff H, Bracker TU, Henderson D, Politz O (2007). MS-275, a potent orally available inhibitor of histone deacetylases—the development of an anticancer agent. *Int J Biochem Cell Biol* 39, 1388–1405.
- Hu E, Dul E, Sung C-M, Chen Z, Kirkpatrick R, Zhang G-F, Johanson K, Liu R, Lago A, Hofmann G, et al. (2003). Identification of novel isoform-selective inhibitors within class I histone deacetylases. *J Pharmacol Exp Ther* 307.2, 720–728.
- Hu G, Agarwal P (2009). Human disease-drug network based on genomic expression profiles. *PLoS One* 4, e6536.
- Hubbert C, Guardiola A, Shao R, Kawaguchi Y, Ito A, Nixon A, Yoshida M, Wang X-F, Yao T-P (2002). HDAC6 is a microtubule-associated deacetylase. *Nature* 41, 455–458.
- Hughes B (2010). 2009 FDA drug approvals. *Nat Rev Drug Discov* 9.2, 89–92.
- Ignashkova TI, Gendarme M, Peschk K, Eggenweiler H-M, Lindemann RK, Reiling JH (2017). Cell survival and protein secretion associated with Golgi integrity in response to Golgi stress-inducing agents. *Traffic* 530–544.
- Iorio F, Bosotti R, Scacheri E, Belcastro V, Mithbaokar P, Ferriero R, Murino L, Tagliaferri R, Brunetti-Pierri N, Isacchi A, et al. (2010). Discovery of drug mode of action and drug repositioning from transcriptional responses. *Proc Natl Acad Sci USA* 107.33, 14621–14626.
- Iorio F, Tagliaferri R, di Bernardo D (2009). Identifying network of drug mode of action by gene expression profiling. *J Comput Biol* 16.2, 241–251.
- Kamal A, Hussaini SMA, Rahim A, Riyaz S (2015). Podophyllotoxin derivatives: a patent review (2012–2014). *Expert Opin Ther Pat* 25.9, 1025–1034.
- Kelland L (2007). Broadening the clinical use of platinum drug-based chemotherapy with new analogues: satraplatin and picoplatin. *Expert Opin Invest Drugs* 16.7, 1009–1021.
- Khabele D, Son D-S, Parl AK, Goldberg GL, Augenlicht LH, Mariadason JM, Rice VM (2007). Drug-induced inactivation or gene silencing of class I histone deacetylases suppresses ovarian cancer cell growth: implications for therapy. *Cancer Biol Ther* 6.5, 795–801.
- Khan N, Jeffers M, Kumar S, Hackett C, Boldog F, Khramtsov N, Qian X, Mills E, Berghs SC, Carey N, et al. (2008). Determination of the class and isoform selectivity of small-molecule histone deacetylase inhibitors. *Biochem J* 409, 581–589.
- Lamb J (2006). The connectivity map: using gene-expression signatures to connect small molecules, genes, and disease. *Science* 313, 1929–1935.
- Lamb J (2007). The connectivity map: a new tool for biomedical research. *Nat Rev Cancer* 7, 54–60.
- Lane JD, Lucocq J, Pryde J, Barr FA, Woodman PG, Allan VJ, Lowe M (2002). Caspase-mediated cleavage of the stacking protein GRASP65 is required for Golgi fragmentation during apoptosis. *J Cell Biol* 156, 495–509.
- Laubach JP, Moreau P, San-Miguel JF, Richardson PG (2015). Panobinostat for the treatment of multiple myeloma. *Clin Cancer Res* 21, 4767–4773.
- Lee H-Z, Kwitkowski VE, Del Valle PL, Ricci MS, Saber H, Habtemariam BA, Bullock J, Bloomquist E, Shen YL, Chen X-H, et al. (2015). FDA approval: belinostat for the treatment of patients with relapsed or refractory peripheral T-cell lymphoma. *Clin Cancer Res* 21, 2666–2670.
- Lee JJ, Beumer JH, Chu E (2016). Therapeutic drug monitoring of 5-fluorouracil. *Cancer Chemother Pharmacol* 78, 447–464.
- Li J, Deffieux MS, Lee PL, Saha P, Pfeffer SR (2015). Glycosylation inhibition reduces cholesterol accumulation in NPC1 protein-deficient cells. *Proc Natl Acad Sci USA* 112, 14876–14881.
- Liberali P, Snijder B, Pelkmans L (2014). A hierarchical map of regulatory genetic interactions in membrane trafficking. *Cell* 157, 1473–1487.
- Machamer CE (2015). The Golgi complex in stress and death. *Front Neurosci* 9, 1–5.
- Mackmull M-T, Iskar M, Parca L, Singer S, Bork P, Ori A, Beck M (2015). Histone deacetylase inhibitors (HDACi) cause the selective depletion of bromodomain containing proteins (BCPs). *Mol Cell Proteom* 14, 1350–1360.
- Manal M, Chandrasekar MJN, Jeyapal Gomathi P, Nanjan MJ (2016). Inhibitors of histone deacetylase as antitumor agents: a critical review. *Bioorg Chem* 67, 18–42.
- Mann BS, Johnson JR, Cohen MH, Justice R, Pazdur R (2007). FDA approval summary: vorinostat for treatment of advanced primary cutaneous T-cell lymphoma. *Oncologist* 12, 1247–1252.
- Mazur PK, Herner A, Mello SS, Wirth M, Hausmann S, Sánchez-Rivera FJ, Lofgren SM, Kuschma T, Hahn SA, Vangala D, et al. (2015). Combined inhibition of BET family proteins and histone deacetylases as a potential epigenetics-based therapy for pancreatic ductal adenocarcinoma. *Nat Med* 21, 1163–1171.
- Miller KM, Tjeertes JV, Coates J, Legube G, Polo SE, Britton S, Jackson SP (2010). Human HDAC1 and HDAC2 function in the DNA-damage response to promote DNA nonhomologous end-joining. *Nat Struct Mol Biol* 17, 1144–1151.
- Mottet D, Bellahcene A, Pirotte S, Waltregny D, Deroanne C, Lamour V, Lidereau R, Castronovo V (2007). Histone deacetylase 7 silencing alters endothelial cell migration, a key step in angiogenesis. *Circ Res* 101, 1237–1246.
- Nervi C, De Marinis E, Codacci-Pisanelli G (2015). Epigenetic treatment of solid tumours: a review of clinical trials. *Clin Epigenet* 7, 127–147.
- Oku M, Tanakura S, Uemura A, Sohma M, Misumi Y, Taniguchi M, Wakabayashi S, Yoshida H (2011). Novel cis-acting element GASE regulates transcriptional induction by the Golgi stress response. *Eng Cell Struct Funct* 36, 1–12.
- Otsu N (1979). A threshold selection method from gray-level histograms. *IEEE Trans Syst Man Cybern* 9, 62–66.
- Pan H, Yu J, Zhang L, Carpenter A, Zhu H, Li L, Ma D, Yuan J (2008). A novel small molecule regulator of guanine nucleotide exchange activity of the ADP-ribosylation factor and golgi membrane trafficking. *J Biol Chem* 283, 31087–31096.
- Pearl MJ, Smyth GK, van Laar RK, Bowtell DD, Richon VM, Marks PA, Holloway AJ, Johnstone RW (2005). Identification and functional significance of genes regulated by structurally different histone deacetylase inhibitors. *Proc Natl Acad Sci USA* 102, 3697–702.
- Petri S, Meister G (2013). Target identification and validation in drug discovery. *Methods Mol Biol* 986, 59–71.
- Petrosyan A (2015). Onco-Golgi: is fragmentation a gate to cancer progression? *Biochem Mol Biol J* 1, 1477–1490.
- Peyroche A, Antony B, Robineau S, Acker J, Cherfils J, Jackson CL (1999). Brefeldin A acts to stabilize an abortive ARF-GDP-Sec7 domain protein complex: involvement of specific residues of the Sec7 domain. *Mol Cell* 3, 275–285.
- Picaud S, Wells C, Felletar I, Brotherton D, Martin S, Savitsky P, Diez-Dacal B, Philpott M, Bountra C, Lingard H, et al. (2013). RVX-208, an inhibitor of BET transcriptional regulators with selectivity for the second bromodomain. *Proc Natl Acad Sci USA* 110, 19754–19759.
- Reiling JH, Olive AJ, Sanyal S, Carette JE, Brummelkamp TR, Ploegh HL, Starnbach MN, Sabatini DM (2013). A CREB3-ARF4 signaling pathway mediates the response to Golgi stress and susceptibility to pathogens. *Nat Cell Biol* 15, 1473–1485.
- Sáenz JB, Sun WJ, Chang JW, Li J, Bursulaya B, Gray NS, Haslam DB (2009). Golgicide A reveals essential roles for GBF1 in Golgi assembly and function. *Nat Chem Biol* 5, 157–165.
- Scherf U, Ross DT, Waltham M, Smith LH, Lee JK, Tanabe L, Kohn KW, Reinhold WC, Myers TG, Andrews DT, et al. (2000). A gene expression database for the molecular pharmacology of cancer. *Nat Gen* 24, 236–244.
- Sciaky N, Presley J, Smith C, Zaal KJM, Cole N, Moreira JE, Terasaki M, Siggia E, Lippincott-Schwartz J (1997). Golgi tubule traffic and the effects of brefeldin A visualized in living cells. *J Cell Biol* 139, 1137–1155.

- Scott KL, Kabbarah O, Liang M-C, Ivanova E, Anagnostou V, Wu J, Dhakal S, Wu M, Chen S, Feinberg T, et al. (2009). GOLPH3 modulates mTOR signalling and rapamycin sensitivity in cancer. *Nature* 459, 1085–1090.
- Shahbazi J, Liu PY, Atmadibrata B, Bradner JE, Marshall GM, Lock RB, Liu T (2016). The bromodomain inhibitor JQ1 and the histone deacetylase inhibitor panobinostat synergistically reduce N-Myc expression and induce anticancer effects. *Clin Cancer Res* 22, 2534–2544.
- Song J, Noh JH, Lee JH, Eun JW, Ahn YM, Kim SY, Lee SH, Park WS, Yoo NJ, Lee JY, et al. (2005). Increased expression of histone deacetylase 2 is found in human gastric cancer. *APMIS* 113, 264–268.
- Stengel KR, Hiebert SW (2015). Class I HDACs affect DNA replication, repair, and chromatin structure: implications for cancer therapy. *Antioxid Redox Signal* 23, 51–65.
- Sun B, Shah B, Fiskus W, Qi J, Rajapakshe K, Coarfa C, Li L, Devaraj SGT, Sharma S, Zhang L, et al. (2015). Synergistic activity of BET protein antagonist-based combinations in mantle cell lymphoma cells sensitive or resistant to ibrutinib. *Blood* 126, 1565–1574.
- Sütterlin C, Hsu P, Mallabiabarrena A, Malhotra V (2002). Fragmentation and dispersal of the pericentriolar Golgi complex is required for entry into mitosis in mammalian cells. *Cell* 109, 359–369.
- Taniguchi M, Nadanaka S, Tanakura S, Sawaguchi S, Midori S, Kawai Y, Yamaguchi S, Shimada Y, Nakamura Y, Matsumura Y, et al. (2015). TFE3 is a bHLH-ZIP-type transcription factor that regulates the mammalian Golgi stress response. *Cell Struct Funct* 40, 13–30.
- Terasawa K, Tomabechei Y, Ikeda M, Ehara H, Kukimoto-Niino M, Wakiyama M, Podyma-Inoue KA, Rajapakshe AR, Watabe T, Shirouzu M, et al. (2016). Lysosome-associated membrane proteins-1 and -2 (LAMP-1 and LAMP-2) assemble via distinct modes. *Biochem Biophys Res Commun* 479, 489–495.
- Tjeertes JV, Miller KM, Jackson SP (2009). Screen for DNA-damage-responsive histone modifications identifies H3K9Ac and H3K56Ac in human cells. *EMBO J* 28, 1878–1889.
- Touw WG, Bayjanov JR, Overmars L, Backus L, Boekhorst J, Wels M, Sacha van Hijum AFT (2013). Data mining in the life sciences with Random Forest: a walk in the park or lost in the jungle? *Brief Bioinform* 14, 315–326.
- Turner JR, Tartakoff AM (1989). The response of the Golgi complex to microtubule alterations: the roles of metabolic energy and membrane traffic in Golgi complex organization. *J Cell Biol* 109, 2081–2088.
- van der Linden L, van der Schaar HM, Lanke KH, Neyts J, van Kuppeveld FJ (2010). Differential effects of the putative GBF1 inhibitors Golgicide A and AG1478 on enterovirus replication. *J Virol* 84, 7535–7542.
- Wagner LM (2015). Fifteen years of irinotecan therapy for pediatric sarcoma: where to next? *Clin Sarcoma Res* 5, 1–7.
- Wang L, Xie L, Ramachandran S, Lee Y, Yan Z, Zhou L, Krajewski K, Liu F, Zhu C, Chen DJ, et al. (2015). Non-canonical bromodomain within DNA-PKcs promotes DNA damage response and radioresistance through recognizing an IR-induced acetyl-lysine on H2AX. *Chem Biol* 22, 849–861.
- Wilke S, Krausze J, Büsow K (2012). Crystal structure of the conserved domain of the DC lysosomal associated membrane protein: implications for the lysosomal glycolyx. *BMC Biol* 10, 62–77.
- Witt O, Deubzer HE, Milde T, Oehme I (2009). HDAC family: what are the cancer relevant targets? *Cancer Lett* 277, 8–21.
- Xi R, Lee S, Xia Y, Kim T-M, Park PJ (2016). Copy number analysis of whole-genome data using BIC-seq2 and its application to detection of cancer susceptibility variants. *Nucleic Acids Res* 44, 6274–6286.
- Xiang Y, Zhang X, Nix DB, Kato T, Aoki K, Tiemeyer M, Wang Y (2013). Regulation of protein glycosylation and sorting by the Golgi matrix proteins GRASP55/65. *Nat Commun* 4, 1659–1671.
- Xu WS, Parmigiani RB, Marks P (2007). Histone deacetylase inhibitors: molecular mechanisms of action. *Oncogene* 26, 5541–5552.
- Yadav S, Puri S, Linstedt AD (2009). A primary role for Golgi positioning in directed secretion, cell polarity, and wound healing. *Mol Biol Cell* 20, 1728–1736.
- Yan H, Tammara M, Liao S (2016). Collision of trapped topoisomerase 2 with transcription and replication: generation and repair of DNA double-strand breaks with 5' adducts. *Genes* 7, E32.
- Yoon S, Eom GH (2016). HDAC and HDAC inhibitor: from cancer to cardiovascular diseases. *Chonnam Med J* 52, 1.
- Zeidner JF, Karp JE (2015). Clinical activity of alvocidib (flavopiridol) in acute myeloid leukemia. *Leuk Res* 39, 1312–1318.
- Zeng Z, Lin H, Zhao X, Liu G, Wang X, Xu R, Chen K, Li J, Song L (2012). Overexpression of GOLPH3 promotes proliferation and tumorigenicity in breast cancer via suppression of the FOXO1 transcription factor. *Clin Cancer Res* 18, 4059–4069.
- Zhang J, Zhong Q (2014). Histone deacetylase inhibitors and cell death. *Cell Mol Life Sci* 71, 3885–3901.
- Zhao S, Xu W, Jiang W, Yu W, Lin Y, Zhang T, Yao J, Zhou L, Zeng Y, Li H, et al. (2010). Regulation of cellular metabolism by protein lysine acetylation. *Science* 327, 1000–1004.